Redox Cycles, Active Materials, and Reactors Applied to Water and Carbon Dioxide Splitting for Solar Thermochemical Fuel Production: A Review

Stéphane Abanades

energies

MDPI

Review

Redox Cycles, Active Materials, and Reactors Applied to Water and Carbon Dioxide Splitting for Solar Thermochemical Fuel Production: A Review

Stéphane Abanades

Processes, Materials and Solar Energy Laboratory, PROMES-CNRS, 66120 Font-Romeu, France; stephane.abanades@promes.cnrs.fr

Abstract: The solar thermochemical two-step splitting of H_2O and CO_2 based on metal oxide compounds is a promising path for clean and efficient generation of hydrogen and renewable synthetic fuels. The two-step process is based on the endothermic solar thermal reduction of a metal oxide releasing O_2 using a high-temperature concentrated solar heat source, followed by the exothermic oxidation of the reduced oxide with H_2O and/or CO_2 to generate pure H_2 and/or CO. This pathway relates to one of the emerging and most promising processes for solar thermochemical fuel production encompassing green H_2 and the recycling/valorization of anthropogenic greenhouse gas emissions. It represents an efficient route for solar energy conversion and storage into renewable and dispatchable fuels, by directly converting the whole solar spectrum using heat delivered by concentrating systems. This eliminates the need for photocatalysts or intermediate electricity production, thus bypassing the main limitations of the low-efficient photochemical and electrochemical routes currently seen as the main green methods for solar fuel production. In this context, among the relevant potential redox materials, thermochemical cycles based on volatile and non-volatile metal oxides are particularly attractive. Most redox pairs in two-step cycles proceed with a phase change (solid-to-gas or solid-to-liquid) during the reduction step, which can be avoided by using non-stoichiometric oxides (chiefly, spinel, fluorite, or perovskite-structured materials) through the creation of oxygen vacancies in the lattice. The oxygen sub-stoichiometry determines the oxygen exchange capacity, thus determining the fuel production output per mass of redox-active material. This paper provides an overview of the most advanced cycles involving ZnO/Zn, SnO_2/SnO, Fe_3O_4/FeO, ferrites, ceria, and perovskites redox systems by focusing on their ability to perform H_2O and CO_2 splitting during two-step thermochemical cycles with high fuel production yields, rapid reaction rates, and performance stability. Furthermore, the possible routes for redox-active material integration and processing in various solar reactor technologies are also described.

Keywords: solar fuels; water-splitting; CO_2 conversion; thermochemical cycles; redox-active materials; solar reactors; hydrogen and syngas production; metal oxides; non-stoichiometric oxides; oxygen-conducting materials

check for updates

Citation: Abanades, S. Redox Cycles, Active Materials, and Reactors Applied to Water and Carbon Dioxide Splitting for Solar Thermochemical Fuel Production: A Review. *Energies* **2022**, *15*, 7061. https://doi.org/10.3390/en15197061

Academic Editor: Rahul R. Bhosale

Received: 2 September 2022
Accepted: 23 September 2022
Published: 26 September 2022

1. Introduction

New sustainable and alternative energy carriers are required to limit the CO_2 emissions and climate change arising from intensive fossil fuel utilization and combustion. The solar thermochemical production of synthetic fuels without greenhouse gas emission can be achieved via the splitting of H_2O and CO_2, using concentrated solar energy as an external high-temperature heat source for the chemical process [1–3]. The different solar fuels considered consist of hydrogen, syngas (with H_2 and CO as main components), and the derived fuels (including methanol or synthetic liquid fuels derived from Fischer–Tropsch synthesis). Hydrogen is an energy carrier enabling long-term storage and long-range transportation of solar energy and for being used as a fuel in direct combustion engines

or in fuel cells. The utilization of CO_2 emissions captured, e.g., from industrial processes, is also a major challenge, notably for the CO_2 conversion into synthetic fuels driven by solar energy. Accordingly, this can help to contribute in the achievement of global net zero carbon emissions [4] and sustainable development goals (SDGs), in particular related to these actions aiming to ensure access to affordable and clean energy (SDG 7), and to combat climate change (SDG 13). H_2 production and CO_2 conversion/recycling into liquid synthetic fuels can be integrated in industrial processes for the development of an economic sector that would be based on three main industrial components:

(i) Resources and energy harvesting. Though the capture of atmospheric CO_2 by direct air capture (DAC) is not yet at a stage of industrial deployment, several industrial fields already have the potential to supply the required CO_2 for the start-up of this sector, which is rapidly expanding especially with respect to CO_2 capture and sequestration (CCS) [5,6]. H_2O can be extracted from seawater desalination. Finally, regarding the available primary energy sources, concentrated solar energy (CSE) has potential to supply the energy requirements of thermochemical processes.

(ii) H_2O and CO_2 splitting. Among the possible existing paths, photocatalysis and photo-electrolysis appear to be the most challenging to operate at industrial scale, based on the number of constraints related to the relevant materials composing the cells along with the limited solar-to-fuel efficiencies of such processes [7]. Water electrolysis is the most widely developed and commercially available owed to its similarity to hydrogen fuel cells, but more suitable and cost-effective materials are still required. As the major drawback, this pathway remains widely reliant on an inexpensive electricity source, and its coupling with a renewable intermittent energy source (solar or wind power) is considered in the framework of electrical storage of these renewables. Eventually, thermochemical redox cycles based on metal oxides are in an intermediate development stage [8,9]. Their benefits lie in a significantly higher energy efficiency potential because solar heat is directly converted into chemical bond energy, without the need for an intermediate conversion into electrical energy, as required for the electrolysis process.

(iii) Liquid fuel production is definitely the most advanced and developed process of this potentially emerging sector, as it can be based on the Fischer–Tropsch catalytic synthesis, which is an already existing industrial process.

In this review, the various pathways for thermochemical H_2O and CO_2 dissociation are described. Photochemical, photobiological, and electrochemical pathways [10,11] are thus not detailed. Reforming and gasification reactions coupled with solid oxidants (chemical looping processes [12,13]) are also not included because they require an input of hydrocarbon/carbonaceous materials (such as methane or solid carbon/biomass). Among the existing chemical routes, the dissociation (splitting) of H_2O and CO_2 using thermochemical cycles based on metal oxides appears to be the most favorable and energy-efficient pathway [14–16], because concentrated solar energy is directly used as the process heat source, without any intermediate energy losses associated with the production of electricity (case of electrolysis). Furthermore, this route offers a potentially higher energy conversion efficiency (solar-to-fuel) in comparison with direct thermolysis, thanks to a lower temperature, and thereby reduced radiative heat losses. Different types of relevant metal oxide redox cycles and the developed solar reactor technologies for the cycles' implementation in solar processes are presented. In particular, the most advanced and adapted redox systems for H_2O and CO_2 splitting are reviewed. They include (i) volatile or non-volatile oxides with discrete transitions in the metal oxidation state (such as ZnO/Zn, SnO_2/SnO, or Fe_3O_4/FeO) accompanied by a phase change (solid-to-gas or solid-to-liquid) during the reduction step, as well as (ii) non-stoichiometric oxides (including ferrites, ceria, and perovskites redox systems) featuring a continuous redox activity over a variety of temperature and oxygen partial pressure, thanks to vacancies that facilitate oxide ion transport (no crystallographic phase change occurs during redox cycles). The first category involving simple oxides generally produces higher fuel amounts per mass of active material at the expense of recombination issues with O_2 during reduction. In contrast, the absence of

phase change in the second category involving non-stoichiometric oxides eliminates the need for solid reactant transport between steps, but the fuel productivity remains limited due to the low oxygen exchange capacity. The current knowledge related to each of these systems is summarized, while emphasizing their existing advantages and constraints and the most promising reactor technologies applicable for the considered reactions.

2. H_2O and CO_2 Splitting by Direct Thermolysis

Single-step thermolysis corresponds to the dissociation of chemical bonds with oxygen atoms at a high temperature, based on the following reactions:

$$CO_2 \rightarrow CO + \frac{1}{2}O_2 \quad (1)$$

$$H_2O \rightarrow H_2 + \frac{1}{2}O_2 \quad (2)$$

The enthalpy and Gibbs free energy variations as a function of the temperature are displayed in Figure 1 (at atmospheric pressure). The ranges of temperature related to the different considered pathways are also indicated.

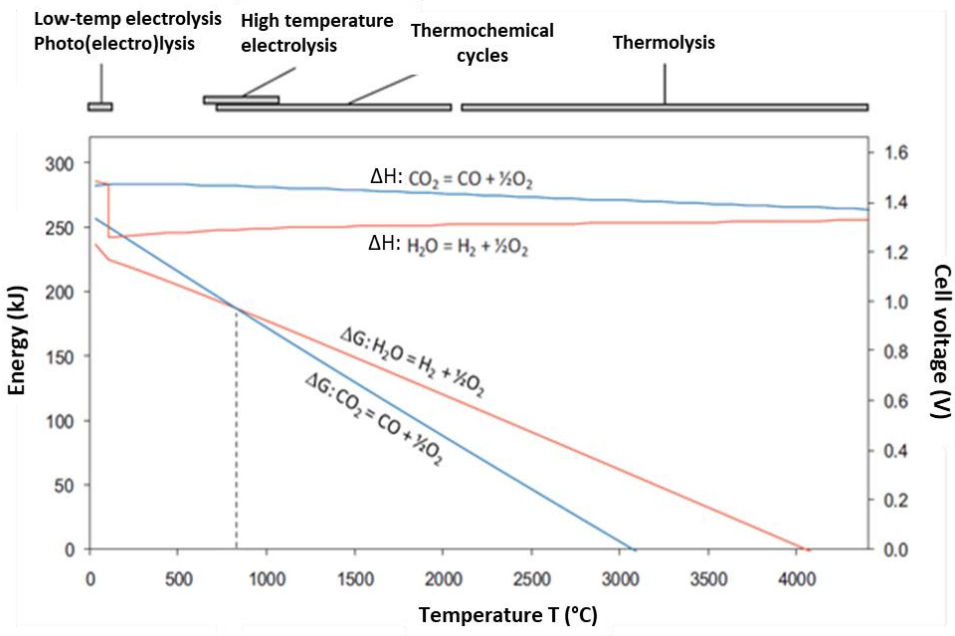

Figure 1. Variation of enthalpy and Gibbs free energy of thermolysis of CO_2 and H_2O as a function of the temperature.

Thermolysis of CO_2 is highly endothermic, and it cannot proceed in a spontaneous way below ~3000 °C. This threshold of temperature is even higher for thermolysis of H_2O. Various simple aspects tend to indicate that operating at such elevated temperatures is not appropriate:

- The design of solar reactors able to withstand repeated thermal constraints is challenging, given that the materials that can potentially be thermally-resistant at such high temperatures are costly and not widely available.
- The reverse reaction (recombination of products) may be avoided, either by the means of H_2 (or CO) and O_2 separation at a very high temperature (thereby avoiding a potentially explosive mixture), or by carrying out a fast quenching of this gaseous species mixture. At present, there does not exist any available technology that would be able to address these points.
- Because radiative heat losses vary with the fourth power of temperature, it is not realistic to achieve high energy conversion efficiencies for this kind of high-temperature process.

- Concentrated solar energy is the only renewable heat source that could be employed to reach such high levels of temperature. However, directly heating a gas (such as H_2O or CO_2) with solar radiation is difficult although these gas species absorb at given wavelengths a fraction of the incident solar spectrum. Therefore, the process complexity has to be increased, for instance, with the addition of particles for promoting absorption and diffusion of solar radiation.

In spite of these issues, Jensen et al. [17] filed a patent on this process relying on the variation of CO_2 absorption spectrum with temperature. Indeed, according to the experimental results, by preheating the gas at 1800 K, solar radiation can be efficiently absorbed in order to drive a CO_2 photolysis into CO, O_2, and O species. The gas mixture can be further cooled down via bulk addition of CO_2 at room temperature in order to generate additional CO by reaction with O. The reported efficiency of CO_2 conversion to CO is ~6%. Such a process cannot be considered as a pure CO_2 thermolysis because concentrated photons trigger the mechanism instead of the temperature effect alone, even though high temperature is required for carrying out the reaction [18,19].

3. H_2O and CO_2 Splitting by Thermochemical Redox Cycles

3.1. Context

A suitable route to overcome the drawbacks associated with direct single-step thermolysis is to decompose this reaction in different steps by using thermochemical multi-step cycles. Proposed for the first time by Funk and Reinstrom [20], this method led to intensive research from laboratories during the first oil crisis in 1973, with the aim to produce hydrogen from water-splitting using the high-temperature heat released by nuclear reactors (~950 °C). The interest in such cycles then declined, but starting with the year 2000, it was actively renewed with the aim to valorize the potential of concentrated solar energy and to provide process heat at high temperatures [21,22].

The cycles most widely studied for high-temperature application (T > 1000 °C) are those composed on reduction and oxidation reactions of metal oxides [23,24]. The two steps involved are: (1) the metal oxide reduction (MO_x) at high temperature, yielding a reduced oxide material and gaseous oxygen (Equation (3)); and (2) the re-oxidation of this compound in the presence of either CO_2 or H_2O, to regenerate the initial metal oxide and produce either CO or H_2 (Equation (4)):

$$MO_x \rightarrow MO_{x-y} + \frac{y}{2}O_2 \; T > 1000\,^{\circ}C, \; \Delta H >> 0 \quad (3)$$

$$MO_{x-y} + yCO_2(H_2O) \rightarrow MO_x + yCO(H_2) \; T < 1000\,^{\circ}C, \; \Delta H < 0 \quad (4)$$

The cost estimation for the H_2 produced with this kind of cycle was in the range 46–66 $/GJ (i.e., 5.5–7.9 $/kg), thus comparable or slightly higher than the cost of electrolysis using nuclear power [25], but with much more favorable prospects of being decreased, owed to the expected drop in solar infrastructure investment costs, as opposed to electricity production costs that will dramatically increase. Depending on assumptions and process scales, different cost ranges were reported for metal oxide-based cycles in various techno-economic analyses (e.g., H_2 production costs in the range 3.5–12.8 €/kg [26], 7.17–19.26 $/kg [27], or 6.68–13.06 €/kg [28], and potentially decreasing to 3.92 $/kg [29] or 2.5 $/kg [30]). Economic prospects are thus favorable for the solar process deployment at industrial scale. It was established that the choice and size of the solar concentrating system, co-generation, and heat recovery are critical to the system efficiency and economic viability of a solar-driven cycle for hydrogen production.

The separate or simultaneous generation of H_2 and CO species enables the on-demand production of a synthetic gas with a controlled H_2:CO mole ratio. This syngas can serve as the building block for the synthesis of methanol [31] or liquid fuels (synthetic hydrocarbon fuels). This synthesis is an essential stage for the development of this path, since it warrants a smooth transition from the current fossil fuel-based economy toward a future economy

based on hydrogen and fuel cells, as well as a means of storage of H_2 in the form of a dispatchable fuel containing high energy density. Indeed, H_2 and CO offer a high energy density by weight, but their energy density by volume is low (as shown in Figure 2 [32], diesel being similar to gasoline and dimethylfuran (DMF) or third generation biofuel).

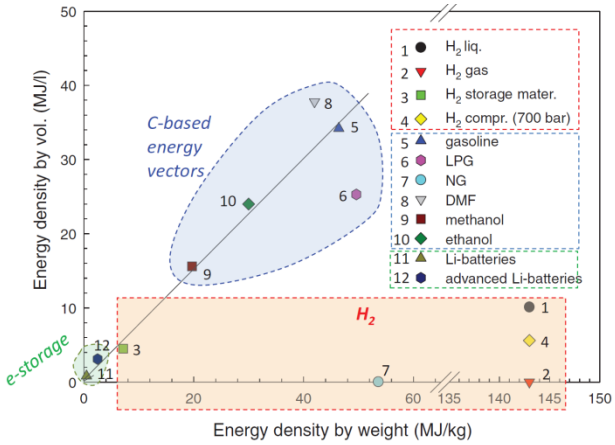

Figure 2. Energy densities by weight and by volume and comparison for different energy carriers.

Once the syngas mixture is produced, the most directly available route to generate liquid hydrocarbon fuels relies on the catalytic Fischer–Tropsch synthesis. This synthesis method has been commercially employed since the 1920s for generating liquid fuels from fossil fuel-derived syngas produced from carbon/coal gasification or from steam natural gas reforming. The Fischer–Tropsch synthesis can be expressed using the following general reaction [33]:

$$2H_2(g) + CO(g) \rightarrow \text{-}CH_2\text{-}\ (l) + H_2O(g) \qquad \Delta H = -165\ kJ/mol \tag{5}$$

where -CH_2- is a link in the hydrocarbon chain. The carbon chain length that determines the fuel quality depends on several factors, including pressure, temperature, and composition of the syngas feedstock, and on the type of catalyst [34,35]. Furthermore, the separate production of the two syngas components makes the precise adjustment of its global composition easier and influences the reaction selectivity to one of the products of the Fischer–Tropsch synthesis. Finally, the poisoning of the catalyst by sulfur is avoided.

Several categories of multi-step cycles can be distinguished, mainly based on the reactions and technology to be implemented for chemical processing [21,27,36–40]. Thermochemical cycles with the number of steps above two offer the advantage of lower operating temperatures, which are compatible with a nuclear heat source, but they require more complicated management of the material flow and transport of reactants and products, additional separation steps, and corrosion issues, which in turn represent strong process limitations [41]. Regarding the two-step cycles, a distinction can be made between the cycles for which the reduction step leads to a partial reduction of the oxide (non-stoichiometric cycles) or a different species (stoichiometric cycle). This species can then be obtained in a gaseous form (cycles with volatile oxides) or not (cycles with non-volatile oxides). Non-stoichiometric cycles have a lower productivity in H_2/CO per unit mass of oxide. As for the cycles with volatile oxides, they generate a gaseous product that easily recombines (with O_2) and must be recovered by condensation and filtration, but whose specific surface area is significant (several dozens of m^2/g) and regenerated at each cycle. Besides these technological criteria, the thermodynamic properties related to these cycles are highly important, as they will determine the maximal efficiencies obtained through theoretical energy/exergy analyses [21,42]. The different sources and wells are represented in Figure 3 showing the mass and energy flow diagrams.

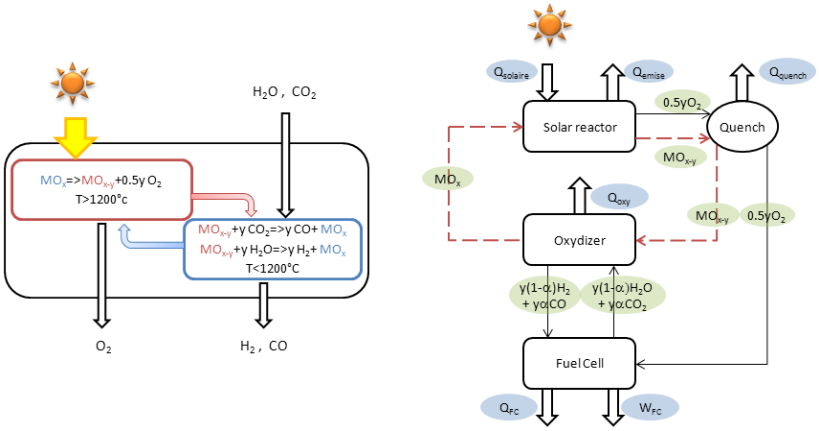

Figure 3. Mass and energy flow diagrams for a typical two-step thermochemical cycle.

Carbon-neutral fuels produced from redox cycles driven by concentrated solar energy have the potential to decarbonize parts of the transportation sector and industrial processes. For providing a sustainable alternative to fossil-derived energy carriers, both the environmental impacts and economic aspects of their production are important. For this purpose, the solar thermochemical fuel production pathways were also characterized based on techno-economic and life-cycle analyses to demonstrate environmental and cost benefits [27,43–45].

3.2. Cycles Based on Volatile Oxides

3.2.1. ZnO/Zn Redox Pair

The two-step ZnO/Zn cycle was widely investigated for its significantly elevated theoretical energy conversion efficiency (conversion efficiency of solar energy into chemical energy ranging from 35% to 50% depending on the extent of heat recovery [46,47]).

The reduction kinetics of ZnO was investigated by using a solar-driven thermogravimetric system [48–50], yielding an activation energy of 361 ± 53 kJ/mol for a temperature of 1800–2100 K and a zero-order reaction. Other solutions were considered [51], especially the reduction in the form of aerosol, which enhances the pre-exponential factor by several orders of magnitude [52,53]. The global efficiency of this step widely depends on the solar heat transfer to the solid reacting particles (direct irradiation is thus preferable) and on the Zn(g) and O_2 separation to avoid their recombination [54]. A rapid gaseous quenching is commonly used as the relevant solution (Zn vaporization starts at a temperature of 907 °C followed by its recrystallization based on a heterogeneous mechanism from nucleation sites), though the energy thus released from products can hardly be recovered in the process.

Zinc re-oxidation takes place following two stages encompassing a 1st rapid stage corresponding to the available zinc surface oxidation, followed by a 2nd longer stage limited by diffusion inside zinc particles (resulting in particle surface passivation). The particle size thus directly impacts the reaction rate, as fine particles will limit the effect of the diffusion mechanism [55–57]. In the case of an oxidation step with only H_2O [58,59] or CO_2 [60,61], the gas oxidant concentration shows a weak influence on the reaction kinetics, in contrast to temperature. The main different characteristics between the oxidation reactions with H_2O and CO_2 are related to the kinetics: the activation energies of the oxidation step were determined to be respectively 87.7 ± 7 kJ/mol [55] and 162 ± 25.3 kJ/mol [62] for similar particles. Despite this strong difference, the co-splitting of H_2O and CO_2 was investigated [63]. A close connection between the inlet gas composition and the generated syngas quality was evidenced. The oxidation of gaseous Zn by either CO_2 or H_2O was studied [64], showing a 10 times increase in the kinetics in comparison with solid Zn particles. The heterogeneous oxidation of Zn(g) provides rapid conversion of Zn to ZnO [65,66]. In spite of this performance, the application of this method is unlikely,

because its implementation is difficult. Though it is produced in the gaseous phase during the reduction step, Zn vapor must be condensed to avoid its recombination and enable its separation from O_2 (thus only solid Zn is available for the oxidation step), while the released energy during its condensation cannot be recovered and is thus lost via the gas quenching.

The main challenges of this cycle highlighted from previous works are:

- The reduction step temperature is elevated (above 2000 K).
- The quenching of gases from >2000 K to >1200 K is a key step during the reduction: its efficiency is decisive for the zinc oxidation step (depending on both size of zinc particles and purity) and global process energy efficiency.
- The re-oxidation step is limited by a passivation phenomenon arising from the formation of a ZnO layer at the particle surface.

The carbon species addition to zinc oxide can be considered in order to decrease the temperature of the reduction step (carbothermal reduction). Indeed, carbon is a reducing agent that helps to facilitate the reaction with the generation of CO in the first step [67]. The first step of the cycle thus becomes:

$$ZnO(s) + C \rightarrow Zn(g) + CO,\ \Delta G\ <\ 0 \text{ for } T\ >\ 1230\ K \quad (6)$$

The studied carbonaceous sources were methane [68–71] and carbon/coals [72–74] (graphite, activated carbon, charcoal, petroleum coke, etc.) or biomass [75,76]. The type of carbon is essential for the reduction step, and charcoal and activated carbon were shown to be good reducing agents. The retained reaction mechanism consists of two successive solid–gas reactions [77]:

$$ZnO(s) + CO \rightarrow Zn(g) + CO_2 \quad (7)$$

$$CO_2 + C(s) \leftrightarrow 2CO \quad (8)$$

3.2.2. SnO_2/SnO Redox Pair

Since elemental tin can be in the form of different oxidation states, +II or +IV, several redox pairs can be considered including SnO_2/SnO, SnO_2/Sn, and SnO/Sn. A first cycle scheme composed of three steps was patented by D. Souriau in 1971, with the aim to valorize the heat released by a nuclear reactor as an energy source. The cycle involves the high-temperature SnO_2 reduction into SnO (Equation (9)), which disproportionates at 600 °C into liquid metallic Sn and SnO_2 (Equation (10)). Then, liquid Sn reacts with H_2O to produce H_2 and regenerate the tin dioxide (Equation (11)):

$$SnO_2 \rightarrow SnO + \frac{1}{2}O_2 \quad (9)$$

$$2SnO \rightarrow Sn(l) + SnO_2 \quad (10)$$

$$Sn(l) + 2H_2O \rightarrow SnO_2 + 2H_2 \quad (11)$$

In a study performed by Charvin et al. [78], the formation of the two phases was not observed although dismutation occurred, which hinders the recovery of Sn(l) in liquid phase, and thus the remaining steps of the cycle become caducous. Since then, the SnO_2/SnO cycle was rather considered and developed [79–81]: the 1st step corresponds to the same reaction of Souriau cycle, while the 2nd one bypasses the disproportionation step and directly employs SnO as the reducing agent:

$$SnO_2 \rightarrow SnO(g) + \frac{1}{2}O_2 \quad (12)$$

$$SnO + \alpha CO_2 + (1-\alpha)H_2O \rightarrow SnO_2 + \alpha CO + (1-\alpha)H_2, 0 < \alpha < 1 \quad (13)$$

Metallic tin was indeed shown to not be necessarily more reactive than SnO for water splitting [78]. This cycle was patented by PROMES for the production of H_2 (WO 2008113944).

Similar to ZnO/Zn cycle, products recombination is limiting for the reduction step efficiency [54]. Decreasing the total pressure in the reaction chamber facilitates the gaseous species production, according to Le Chatelier's principle, and enables a decrease in the temperature required for the reaction (1900 K at 20 kPa versus a theoretical temperature of 2342 K at atmospheric pressure). The gas species dilution by using a neutral gas can also be considered in order to decrease the O_2 partial pressure and therefore to limit products recombination. Similarly, the temperature required for the reduction reaction is also decreased. Finally, a rapid gas quenching allows the SnO condensation and the decrease in the gas temperature below the reaction temperature. The condensation mechanism follows a heterogeneous process from the nucleation sites. As for ZnO, the use of carbon as reducer lowers the reduction temperature of SnO_2 [82].

During the re-oxidation step, several parameters should be considered. The composition of the reduced oxide powder (content in reduced tin species) may vary according to the operating conditions (SnO or Sn/SnO_2). Indeed, partial SnO disproportionation may occur during the temperature increase in the oxidation step or during the cooling stage in the first reduction step [81]. Similarly, the powder morphology plays a major role (particle size, specific surface area) because the re-oxidation reaction is a solid–gas reaction. From this viewpoint, the SnO recovery by vapor condensation favors the formation of powders composed of grains with size of the order of several dozen nanometers, which results in a significantly high specific surface area [80]. Finally, the CO_2 or H_2O splitting is not following the same kinetic rates [80]. H_2O starts to be reduced from 525 °C with an activation energy of 51 ± 7 kJ/mol, while CO_2 is only reduced from 700 °C, with an activation energy of 88 ± 7 kJ/mol.

SnO_2/SnO cycle offers several advantages compared to the ZnO/Zn cycle [79]:

- The reduction step temperature is below the one of the ZnO/Zn cycle and could be further decreased by a total pressure decrease inside the reaction chamber. In addition, the decrease in the operating temperature directly results in a higher energy efficiency [83] and thus a more favorable economic viability of the process.
- The dissociation rate of the oxide is significant and is less impacted by the gas quenching stage at the reactor outlet in comparison with zinc oxide (a product with 72% purity is obtained, against 48% for ZnO [84]). Indeed, the zinc boiling point is 907 °C, while that of SnO is 1425 °C; then, prompt condensation of the latter is facilitated.
- Eventually, SnO is a reactive compound for steam reduction.

3.3. Cycles Based on Non-Volatile Oxides

The cycles based on non-volatile oxides offer the advantage of avoiding the formation of gaseous species during the reduction step. This eliminates the need for any transportation of the solid between cycle steps, and both reduction and hydrolysis reactions can be conducted in the same reactor while only alternating the temperature, provided that the phase change (melting) does not occur. The first proposed non-volatile oxide cycle was the iron oxides-based cycle (involving magnetite/wüstite phase transition). The magnetite phase (Fe_3O_4) can be reduced at a temperature of 2100 K and is thus in a liquid phase (melting point at 1811 K). The hydrolysis step starts at a minimum temperature of 450 K [85]. Experimental studies have demonstrated a complete reduction under inert gas, while the reactivity of the hydrolysis step is high, although it is still limited due to passivation caused by the formation of a surface oxide layer [86–88]. Furthermore, the experimental studies revealed the beneficial effect of quenching after magnetite reduction to avoid the wüstite dismutation into metallic iron and magnetite below a temperature of 570 °C. The theoretical energy efficiency for this cycle is estimated at 35% (based on the higher heating value HHV of H_2).

$$Fe_3O_4 \rightarrow 3FeO + \frac{1}{2}O_2 \quad (14)$$

$$3FeO + H_2O \rightarrow Fe_3O_4 + H_2 \quad (15)$$

In order to decrease the cycle temperature, mixed oxide compounds (based on M_3O_4/MO redox pair) were developed and investigated, involving the formation of a solid solution of iron oxide, offering both a higher reducibility at lower temperature and a better thermal stability of the material that remains in solid phase throughout the cycle [89]. The $M_xFe_{3-x}O_4/M_xFe_{1-x}O$ redox pair thus obtained can indeed be reduced at a lower temperature than pure Fe_3O_4, and the material remains in the solid phase during the high-temperature step. The metallic dopant is incorporated in the magnetite spinel structure, thus forming a ferrite material. The reduction step is further facilitated by such a doping because it creates a structural deformation in the structure of the spinel, thus favoring oxygen mobility. A variety of dopants were investigated, including Mg, Mn, Co, Ni, Cu, and Zn. Iron oxides dissolved within YSZ matrix also showed improved reactivity [90].

Another cycle relies on the CeO_2/Ce_2O_3 system [91]. The reactions of the two-step cycle are comprising the thermal reduction step of Ce^{4+} into Ce^{3+} and the hydrolysis step of Ce^{3+} with steam (or CO_2).

$$2CeO_2 \rightarrow Ce_2O_3 + \frac{1}{2}O_2 \quad (16)$$

$$Ce_2O_3 + H_2O\ (CO_2) \rightarrow 2CeO_2 + H_2\ (CO) \quad (17)$$

When heating above about 1950 °C under reduced pressure, a complete reduction extent to Ce^{3+} can be achieved in liquid phase. Then, in the next oxidation step (hydrolysis), Ce_2O_3 features both a high reactivity (with complete oxidation conversion) and a fast kinetic rate from ~400 °C (e.g., complete Ce_2O_3 re-oxidation to CeO_2 in about 5 min in comparison with about 30% conversion in 2 h for FeO oxidation), and the particle's size does not have a significant influence due to the facilitated oxygen diffusion in the ceria crystalline lattice. However, the reduction step temperature of the cycle remains elevated, and a partial CeO_2 sublimation occurs during heating; the theoretical energy efficiency of this cycle is ~40%. A variant three-step cycle based on Ce^{4+}/Ce^{3+} redox pair was also proposed involving mixed cerium oxides (e.g., with pyrochlore structure $Ce_2Si_2O_7$ or $Ce_2Ti_2O_7$ [92]). As described in the next section related to non-stoichiometric (and non-volatile) oxides, doping strategies of ceria with another secondary metal ($Ce_xM_{1-x}O_2$) can help to improve the ceria reduction rate by creating oxygen vacancies (oxygen sub-stoichiometry), thus enabling the O_2-releasing step to be conducted at a lower temperature [93–95].

3.4. Cycles Based on Non-Stoichiometric Oxides

3.4.1. Cycles Based on Ferrites

The first research investigations on the topic of non-stoichiometric oxides were related to ferrite systems [89], which are among the most advanced systems to have been tested to the stage of a 100 kW (thermal) pilot-scale demonstrator [96]. The Fe_3O_4/FeO two-step cycle is complicated to be implemented as such. On the one hand, the required temperature for thermal reduction of Fe_3O_4 is very high and above the oxide melting point, hence the reduction reaction proceeds in liquid phase (FeO melting point is 1377 °C). The FeO product then requires a milling to obtain a fine powder in order to warrant a sufficient specific surface area for the oxidation step. Furthermore, the produced FeO species disproportionates into Fe_3O_4 and metallic Fe above 570 °C, and therefore the quenching of the product below this temperature is required. A proposed approach to overcome these issues is the substitution of some iron atoms in the crystalline lattice with other metals. As such, the idea of this method is to insert metals that are more readily reducible, although being less reactive to the oxidant (steam or CO_2) than metallic iron (case of Co, Ni, Mn, etc.). Thus, the resulting ferrites with inserted dopants (with $(Fe_{1-x}M_x)_3O_4$ formula, where M = Mg, Mn, Co, Ni, Zn, etc.) still remain reactive to the oxidizing agents such as water, while they can be partially reduced to a $(Fe_{1-x}M_x)_3O_{4-\delta}$ non-stoichiometric form at much lower temperatures than Fe_3O_4.

On the basis of the numerous research studies performed on this topic, nickel-based ferrites appear to offer the best performances in terms of fuel production yield and thermo-

chemical stability with a reduction step temperature maintained below ~1400–1500 °C [97–99]. Nevertheless, ferrites usually do not have a sufficient cycling stability because of unavoidable sintering and induced losses of redox activity and fuel production capacity. To avoid this phenomenon, the coating of the active phase on a ceramic inert support was widely considered [100,101]. The studies revealed that the best-performing substrates include yttrium-stabilized zirconia (YSZ) [102] and monoclinic zirconia (m-ZrO_2) [103], but the reduction rates remain below 30%. Given that the substrate may account for 90 wt% of the mass of the reacting material, the mass-specific H_2 productivity (mole of H_2 per mass of involved material) for this kind of solution remains weak.

3.4.2. Cycles Based on Ceria

Cerium dioxide or ceria (CeO_2) is used widely in the automobile industry as a catalytic material for oxidizing the exhaust gases to permit abatement of gaseous pollutants. This application relies on the facilitated solid-state diffusion and exchange of oxygen ion in the ceria crystalline lattice, which is also advantageous for the reduction and oxidation steps of thermochemical cycles [104,105]. The first study on ceria redox cycle for fuel production was conducted in 2006 by Abanades and Flamant [91]. When decreasing the reduction step temperature of ceria, only a partial reduction of Ce^{4+} in ceria occurs (oxygen vacancies are thus created via a non-stoichiometric reduction), which relates to the $CeO_2/CeO_{2-\delta}$ redox pair system [106–110]. In brief, for pure ceria, the reduction extent remains low, and it is controlled chiefly by the heating rate used to reach the reduction temperature (the maximum oxygen non-stoichiometry δ at equilibrium is determined by the operating temperature under a fixed oxygen partial pressure), which limits the overall fuel productivity per cycle, but the rapid oxidation kinetics make it possible to consider a large number of redox cycles during sunny periods.

The reduction capacity of the ceria-based material can be further enhanced if ceria is doped with aliovalent or tetravalent cationic elements [111–119]. Various studies focused on the proposal of new formulations for doped ceria, including their chemical synthesis and testing implementation and have, for instance, demonstrated the benefit of doping with Zr^{4+} ($Ce_xZr_{1-x}O_2$) [120–122]. By comparison, the previously investigated Ni-doped ferrites yielded a maximum fuel production of 250 $\mu mol/g_{oxide}$, against 333 $\mu mol/g_{oxide}$ for ceria-zirconia mixed oxide, and the latter was more efficient in terms of kinetics of H_2 production and cycling stability.

Various ceria doping and shaping strategies were described [94] and showed their strong effects on the ceria redox cycle performances. The structure and morphology of the material is of prime importance, as it may affect the high-temperature material stability [94,123–126]. These two important properties are dependent on the methods involved during the material synthesis (e.g., as a powder) and its a posteriori shaping and structuring. An attractive concept for material shaping has recently been assessed, consisting in using ceria in the form of porous structures (e.g., reticulated open-cell foams with a dual-scale porosity) [127–129]. The porosity at the macroscopic scale is useful for the efficient volumetric heating of the whole reacting material, which can be itself micro-structured to enhance the specific surface area inside the struts (solid–gas interface area) [130,131]. The elaboration of three-dimensionally ordered macroporous structures (3DOM) using biomimetic approaches has also been considered (e.g., cork-templated or wood-templated ceria) [132–135].

Despite various recent advances in the field, several aspects can still be developed in order to plainly take profit of the advantages of ceria-based redox cycles:

- The ceria formulations can further be optimized (incorporation of several new dopants, utilization of composite materials [136], etc.).
- When the material is used in the form of a powder, the considered synthesis methods warranting high-temperature material resistance must be preferred.
- When the reacting material is structured (porous architecture), thermally-resistant supports (substrates) and efficient coating methods are needed. Alternatively, original

methods need to be developed for the elaboration of architectured porous structures (e.g., biomimetics, 3D printing, etc.) [137–142].

3.4.3. Cycles Based on Perovskites

The perovskite structure is generally related to the ABO_3 compounds, where A and B are cations (B cation size is smaller than that of A). In addition, A and B cations are bonded to twelve and six oxygen atoms, respectively (Figure 4a). The main advantage of such a structure is that the substitution of some A and B sites with other cations is possible and this may alter the structural stability by creating defects. Hence, these substitutions make it possible to generate compounds of $A_{1-x}A'_xB_{1-y}B'_yO_3$ type ($0 < x,y < 1$) and to finely adjust their thermochemical properties, as required in redox cycles [9,143–146].

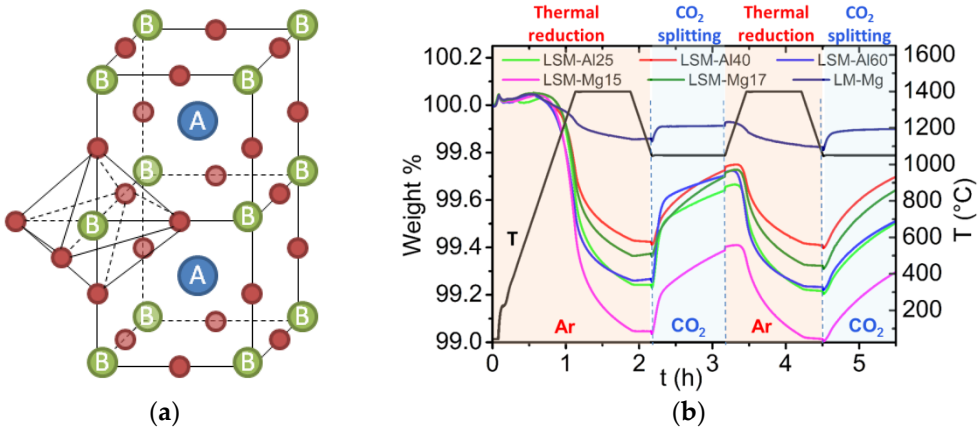

(**a**) (**b**)

Figure 4. Perovskite-based cycles: (**a**) Scheme of ABO_3 perovskite structure; (**b**) Reduction and re-oxidation cycles involving $La_xSr_{1-x}MnO_3$ (LSM) perovskites substituted with either Al or Mg in the B site (2 successive cycles, reduction in Ar at 1400 °C and oxidation in 50% CO_2 at 1050 °C).

By precisely selecting the cations filling the A and B sites and the doping elements, structural deformations can possibly be obtained, as well as modifications of the crystal electronic configuration, which may promote the migration/diffusion of the oxygen and thus facilitate its release from the material. The combination of this attractive property with the electronic stability of the structure is useful to achieve significant oxygen sub-stoichiometry [147–154]. Perovskites with tunable reduction capacities and oxygen ion diffusion rates that are superior to those of ferrites and ceria-based systems can thus be proposed [155–165].

The effect of different dopants on the oxygen evolution and carbon dioxide splitting abilities of lanthanum manganite perovskites was discussed [166,167]. Perovskite formulations such as $La_xSr_{1-x}MnO_3$ (LSM) and variants with A and B site doping were studied [168–176] (production of H_2 or CO higher than ~200 µmol/g, for a reduction step temperature of 1400 °C, as illustrated in Figure 4b), confirming a fuel production capacity potentially higher than the one measured for ceria [177–179]. These performances remain close to those measured for substituted ceria (e.g., ceria-zirconia), but they show promise for a significant potential of material development.

Research works focused on the optimization of the composition and reactivity of materials (perovskite series with A or B site substitutions having a formulation $Ln_{1-x}Ae_xBO_{3-\delta}$) that were synthesized and characterized for the splitting of H_2O or CO_2. For instance, Ca-, Sr-, and Al-doped $SmMnO_3$ [149,150], Ca- and Ga-doped $LaMnO_3$ [151], Ce-substituted $LaSrMnO_3$ [152], $Ce_xSr_{2-x}MnO_4$ [160], $Ca_{0.5}Ce_{0.5}MnO_3$ [159], double-site Ce-substituted $(Ba,Sr)MnO_3$ [180], $La_{0.5}Sr_{0.5}Mn_{1-x}A_xO_3$ (A = Al, Ga, Sc) [163], $SrTi_{0.5}Mn_{0.5}O_{3-\delta}$ [164], $CaTi_{0.5}Mn_{0.5}O_{3-\delta}$ [165], $La_{0.6}Sr_{0.4}Mn_{1-y}Cr_yO_{3-\delta}$ [169,181], Sr- and Mn-doped $LaAlO_{3-\delta}$ [182], $La_{0.4}Sr_{0.6}Mn_{1-x}Al_xO_3$ [183], and $La_{1-x}(Ca,Sr)_xMn_{1-y}Al_yO_3$ [184] are some examples of the numerous materials claimed as potentially attractive candidates for this application. However, the reported performance data have to be considered cautiously because the operating condi-

tions may vary significantly from one material study to another (temperatures, oxygen partial pressures, oxidant concentrations, heating rates, etc.), and performance cannot be directly compared to assess the real capability of the investigated materials. Moreover, apart from the global fuel production output per mass of material, the fuel production rate must also be high enough to warrant both reasonable global cycle duration and high number of cycles performed each sunny day. Unfortunately, the fuel production rates observed in the oxidation step do not compare favorably with pure ceria for most of perovskite formulations investigated to date. However, theoretical calculations showed that perovskites have the potential for improved solar-to-fuel efficiencies during isothermal or near-isothermal redox cycling beyond those achievable by ceria [185].

Kinetic studies were performed to identify the most suitable models of solid–gas reactions for the reduction and oxidation steps [186]. Correlations were also established between geometric parameters of the crystalline structure of perovskites and the redox performances obtained during cycling [187]. In summary, based on the numerous perovskite formulations studied so far, it appears generally that the oxidation kinetics are much lower than for pure ceria, but conversely, the oxygen exchange capacity of considered perovskites (thus the achievable global fuel productivity per mass of material) is higher.

4. Solar Reactor Technologies Developed for Redox Cycles

Two main solar reactor concepts can be proposed to implement redox cycles: the reactors in which both cycle steps can proceed in a single reactor chamber and the reactors in which the functions of reduction and re-oxidation are decoupled in different systems allocated to each step. Concentrated solar heat integration is of prime importance for achieving an optimal solar reactor efficiency [188,189]. The most relevant solar reactor technologies developed to date and applied specifically to two-step cycles are presented.

4.1. Single-Chamber Solar Reactors

This kind of solar reactor gathers the different available technologies for implementing the non-volatile oxide cycles. The reacting material can be either in the form of divided particles (grains or powders of pure material or coated as thin films) or structured with a porous architecture (via the coating of a substrate or by shaping) [190]. In both cases, the target is to offer a large specific surface area for reactions to promote transport phenomena at the solid–gas interfaces.

The possible reactor technological concepts include the fluidized beds with internal particles' circulation, namely circulating fluidized beds (Figure 5). Due to the particles' motion and mixing, a homogenized temperature of the solid can be obtained, the reduction/re-oxidation steps can be performed in alternance, and the particles' sintering can be alleviated. The gas flow is injected in the central part of the cylindrical reactor for the particles' fluidization and for transporting them in the upper region of the bed, so that the upper part of the particle bed is located at the focal point of the solar concentrating system, enabling the reduction reaction. The gas flow-rate is dependent on the particles' size and density that determine the conditions needed for their proper fluidization. When reaching the solar-irradiated zone, the particles return down at the bottom part of the bed via the annular zone at the periphery of the draft tube, thereby transferring a part of the absorbed energy from the top irradiated zone to the bottom zone. An effective thermal homogenization on the vertical axis can be achieved, thus ensuring a more uniform temperature in comparison with packed-beds, and the inert gas flow-rate required for particles' fluidization is restricted to the central region. Once the thermal reduction step is finished, solar irradiation is then stopped, and a fraction of the inlet flow of inert gas is replaced by the oxidizing gas. This reactor concept was, for instance, implemented and operated by using ZrO_2 supporting particles coated with Ni-ferrite ($NiFe_2O_4$) [191].

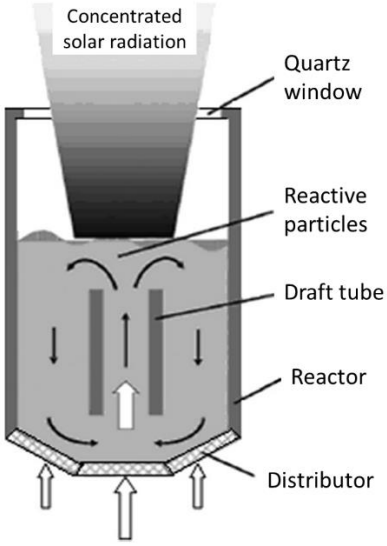

Figure 5. Scheme of a solar-driven fluidized-bed reactor with internal particles circulation.

Another interesting reactor concept consisting of a monolithic reactor was developed, devoted to the solar-driven production of hydrogen fuel, in the framework of a 100 kW (thermal) pilot prototype (Figure 6) [96]. The reacting oxide material (e.g., doped ferrite) is coated on a porous ceramic structure such as honeycomb monolithic, and the whole system acts as both a volumetric radiative absorber and a thermochemical reactor. To allow continuous fuel production during solar operation, two similar parallel reactors are settled in the focal area. While the first one is subjected to concentrated solar radiation for the thermal reduction step, the second one operates the material re-oxidation (ferrite hydrolysis), and vice versa for cycle steps' alternance. Such reactors thus involve a fixed reactant, and the temperature alternance between each step ensures continuous operation via the heliostats' monitoring for control of incident flux.

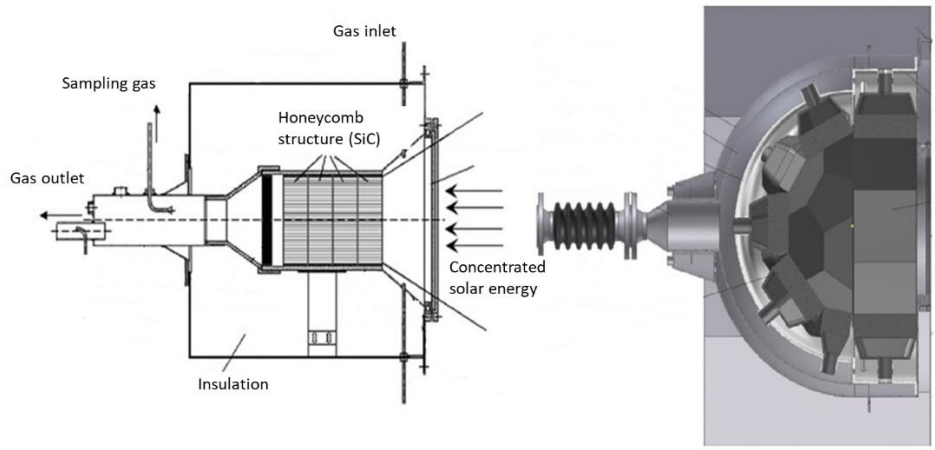

Figure 6. Schemes of monolithic solar reactors integrating a porous structure.

Other types of monolithic solar reactors enabling the integration of massive porous structures made of ceria (monoliths, reticulated foams) have been recently developed (SUNFUEL solar reactor installed at CNRS-PROMES in Figure 7) [130,131,136]. In such reactors, the reactive material is usually cycled at two distinct temperatures for optimized process performance (temperature-swing cycles), although isothermal cycles have also been considered but with much lower fuel production output [114,192–198]. Reticulated porous ceria structures (foams) were prepared by hard templating with a suitable geometry and different pore size densities and then cycled under a wide range of operating conditions (temperatures, O_2 partial pressure, gas flow rates, oxidant mole fraction, H_2O or CO_2

oxidant) in order to determine the material's redox activity. Such foams showed remarkable performances for the splitting of H_2O and CO_2 (fuel production rates up to ~10 mL/min/g) thanks to their dual scale porosity (open cell structure for homogeneous heating and interconnected porosity inside the struts for enhancing the reactivity with the gaseous oxidant species). The cycling stability of materials was assessed during a high number of successive cycles in the reactor under real concentrated solar irradiation conditions [130,131,199]. Ceria foams coated with a thin perovskite layer ($La_{0.5}Sr_{0.5}Mn_{0.9}Mg_{0.1}O_3$) were also elaborated, which allowed an improvement of the global fuel output at the expense of slower oxidation kinetics due to a diffusion barrier at the surface [136]. Moreover, ordered porous structures with a graded porosity (to favor volumetric solar radiation absorption) were designed and manufactured by 3D printing, and their cycling was studied in the solar reactor, which also proved to be effective for the splitting of H_2O and CO_2 [139]. Another shaping strategy was considered consisting of the robocasting of 3D printed and sintered ceria scaffold structures with hierarchical porosity for solar thermochemical fuel production from the splitting of CO_2 [200].

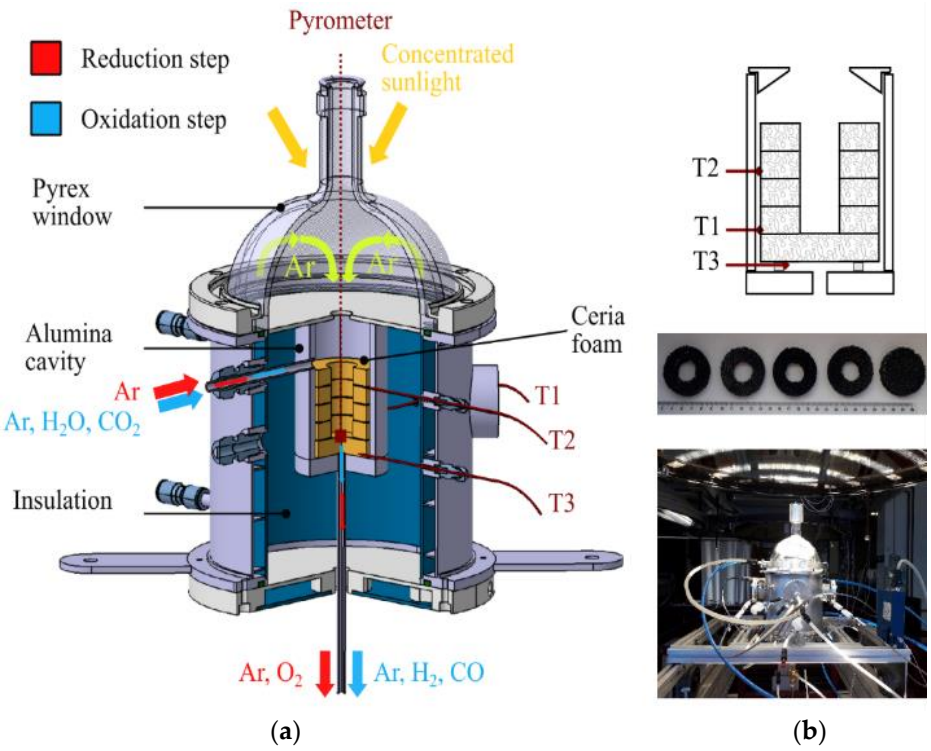

Figure 7. Solar redox cycling of ceria reticulated foams: (**a**) Scheme of the SUNFUEL solar reactor integrating reactive ceria foams for two-step H_2O and CO_2 splitting; (**b**) Foam structure composed of a stack of disc and rings, and pictures after successive cycles performed with a CeO_2 foam under solar heating.

Other alternative shaping strategies were considered in order to integrate the materials in the reactor in a divided form (e.g., particulates). For example, 3-dimensional ordered macroporous (3DOM) ceria materials were synthesized via biomimetics (with cellular ordered microstructure prepared from a cork template, cell diameter ~25 µm). The materials were cycled in different solar reactors with direct or indirect heating [132–134]. Ceria porous microspheres were also elaborated from ion exchange resins and cycled in solar reactors [137], as well as fibrous sintered ceria pellets to demonstrate their suitability for solar fuel production application [140]. The obtained performances were similar to those of ceria foams (~200–300 µmol/g of H_2/CO, peak production rate: 9.5 mL/min/g) under comparable cycling conditions.

Alternatively, a membrane solar reactor was developed for continuous and isothermal splitting of CO_2 (and H_2O) under a gradient of O_2 partial pressure across the membrane [138,201–204]. As described in Figure 8, the original process was demonstrated in a solar reactor under high-flux solar irradiation using a dense ceramic membrane with tubular shape (mixed ionic-electronic conducting materials, MIEC) that separates a reduction zone at low p_{O2} (sweep side) and an oxidation zone fed with reactive gas flow (feed side). The reactive part of the tubular redox membrane was located inside a well-insulated cavity receiver for homogeneous heating, which was fed with a carrier Ar flow on the sweep side to facilitate the transport and removal of the permeated oxygen [138]. The dynamic response of the solar fuel evolution upon varying the operating conditions in the membrane reactor (temperature, CO_2 mole fraction, and feed gas flow rate) was assessed by measuring the evolved gas production rates. Continuous CO_2 dissociation was achieved on the feed side inside the tubular membrane with in situ spatial separation of O_2 and CO across the membrane. The CO and O_2 production rates were sharply enhanced by increasing the operating temperature (up to 1550 °C). The increase in CO_2 concentration or oxidant gas flow rate also enhanced the process performance. Reliable solar membrane reactor operation, under real concentrated sunlight, was successfully demonstrated for the first time, with stable and unprecedented CO production rates up to 0.071 µmol/cm^2/s at 1550 °C and CO/O_2 ratio of 2. An original composite membrane integrating two different perovskite coatings on each side of the ceria membrane, with a sandwich-like structure, was designed and tested under concentrated sunlight [201]. Thin perovskite layers (inner side: $La_{0.5}Sr_{0.5}Mn_{0.9}Mg_{0.1}O_3$ and outer side: $Ca_{0.5}Sr_{0.5}MnO_3$) were coated to enhance oxygen ion transfer. With such a membrane structure, a CO production increase (>0.13 µmol s^{-1} cm^{-2}) and simultaneous oxygen separation (with $CO:O_2$ ratio of 2) were observed, respectively, on the inner and outer sides of the oxygen transport membrane. These results outperform the production rates achieved with uncoated ceria membranes, which demonstrates the interest of using composite membranes made of a densified core material coated with redox-active perovskite layers.

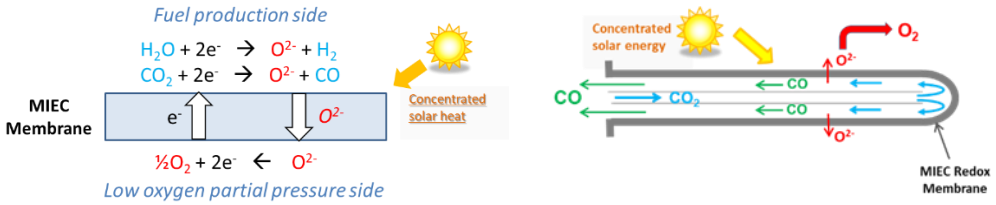

(**a**) (**b**)

Figure 8. Membrane solar reactor: (**a**) Operating principles of the isothermal MIEC membrane with mixed oxygen-electron transfer under a gradient of p_{O2} between both membrane sides; (**b**) Gas flow on the sweep and feed sides, and ion transport through the tubular dense membrane (closed one-end) for continuous separation of oxygen and CO.

4.2. Decoupled Reactors for Separated Reduction and Oxidation Steps

This type of reactor concept is adapted to the cycles in which the reduction step is carried out in a first solar receiver/reactor, and the oxidation step for H_2/CO production is performed separately at a lower temperature in a second oxidation reactor. The heating and cooling stages of the cavity receiver are thus not required, and the solar reactor is specifically designed and optimized for the reduction step. The global system comprising both reactors (solar and oxidation reactors) can potentially be operated in a continuous mode [205]. The most widespread concept relates to the solar reactors devoted to the thermal reduction of volatile oxides.

A prototype reactor with rotating cavity (rotary kiln type) was developed for ZnO dissociation (Figure 9) [206]. Thanks to the cylindrical cavity rotation, the ZnO particles, that are injected by the means of a screw feeding system in the axial region, are evenly distributed and spread on the reactor walls, thus avoiding the existence of hot regions

ascribed to the non-uniform incident solar flux. A permanent inert gas flow is required, and its injection at the rear face of the quartz window allows its protection from Zn vapor deposition. The produced gas species are exiting via the outlet annular section along the screw feeding system, where their cooling/quenching is ensured by the injection of large amounts of inert gas at room temperature (such a quenching method thus consumes inert gas, inducing energy penalties for inert gas separation and recycling). The Zn particles (with ~50% Zn content purity) are finally separated and recovered by filters at the outlet. A different prototype of a rotating solar reactor was also developed at CNRS-PROMES for continuous operation with direct ZnO particles' injection in the high-temperature cavity and Zn product recovery as a fine reactive powder (composed of nanosized particles) at the reactor outlet (Figure 10) [207,208].

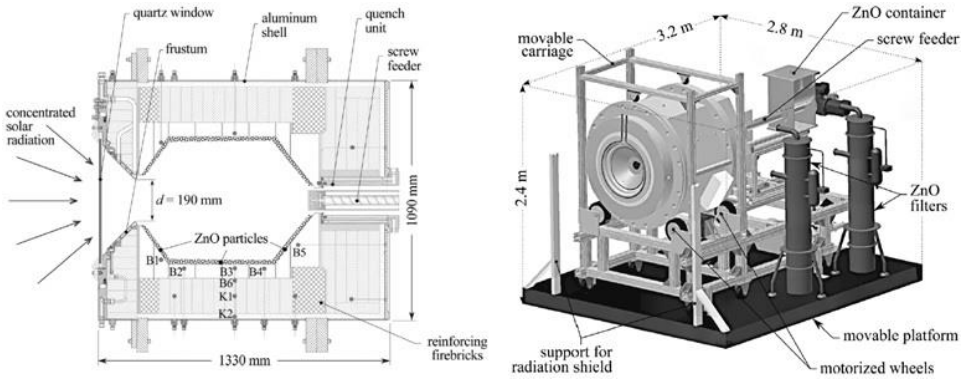

Figure 9. Scheme of 100 kW (thermal) prototype solar reactor for ZnO thermal dissociation.

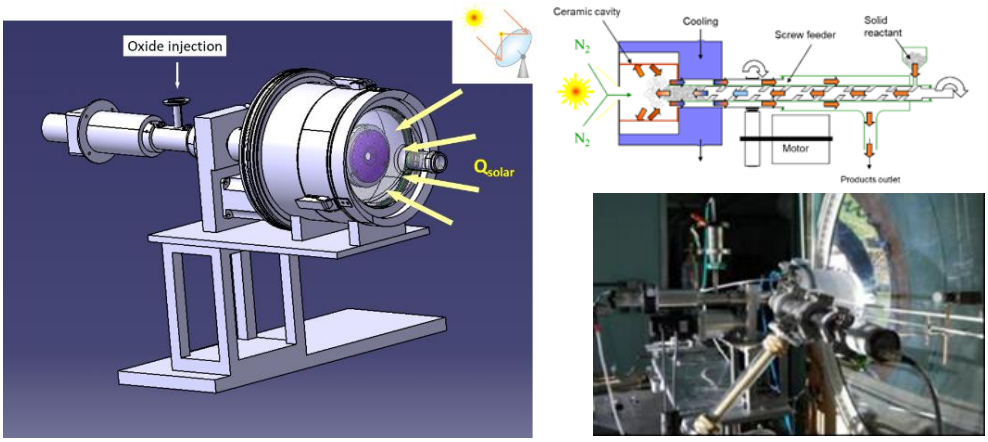

Figure 10. Continuously particle-fed solar reactor for ZnO reduction and Zn production.

The solar reactor prototype with the highest thermal power was developed during the European project Solzinc for the reduction of zinc oxide with carbon materials (Figure 11) [67]. This reactor is thus designed for the carbothermal-reduction of ZnO at lower temperatures (below 1000 °C), which noticeably alleviates the thermal constraints imposed on the reactor materials and the technological issues associated with the gas quenching required in the thermal dissociation process, at the expense of the carbon source requirement. The solar carbothermal reduction of ZnO was mainly studied in shrinking packed-bed reactors, thus based on a similar technology, at smaller scale [77].

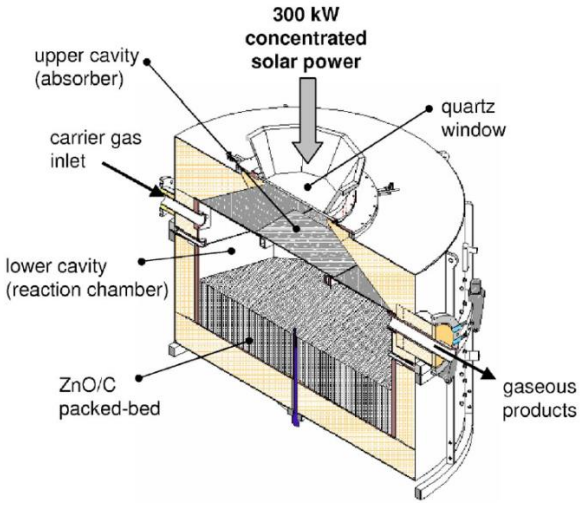

Figure 11. Scheme of the 300 kW (thermal) solar reactor designed for the carbothermal reduction of ZnO.

The considered solar reactor is composed of two separated cavities. The upper cavity of the reactor, composed of SiC plates, acts as the solar receiver, as it receives and absorbs solar irradiation in order to re-emit the energy to the lower cavity that contains a packed-bed of ZnO particles, which are heated by radiations emitted by the separation heat transfer plate. This configuration enables a production of a significant amount of reduced Zn particles without the risk of particles' deposition on the quartz window. The production of 50 kg/h of Zn with 95% purity was achieved, at an operating temperature range of 1300–1500 K, with a process efficiency of 30%.

A different vertical-axis solar reactor concept was developed for the thermal ZnO dissociation (named Gravity Fed Solar Thermochemical Reactor, Figure 12) [209]. In this concept, particles are injected via fifteen distributors located at the periphery of the reactor to homogenize the particles' distribution in the reactor cavity. Driven by gravity, the fed particles fall as a curtain on the surrounding plates made of a refractory material forming the cavity receiver, and the cavity slope and surface were designed for proper operation. The particles are reduced and vaporized zinc is produced during their progress downward in the conical region, while the evolved gases are carried by an inert gas flow to the reactor outlet at the conical cavity bottom. The unreacted particles are then recovered in the annular region located between the gas outlet and the lower part of the reactor.

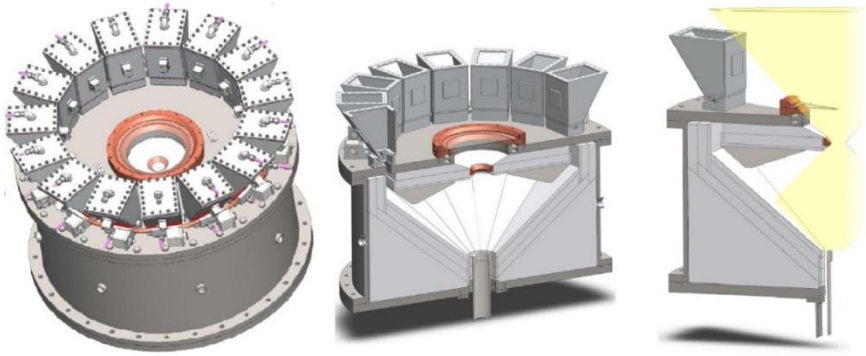

Figure 12. Scheme of the solar reactor with gravity-driven particles injection.

The PROMES laboratory also designed and developed new technological concepts suitable for the continuous thermal reduction of volatile oxides. A first prototype featuring a rotating cavity was assembled, as already shown in Figure 10 [208]. One of the goals and originality of the designed system was the possibility to conduct reactions under reduced

pressure to enhance the kinetics [50,51]. A second different reactor prototype with a vertical solar irradiation axis was then developed, also enabling operation at reduced pressure (Figure 13) [84]. The reacting material, in the form of compressed pellets, is continuously fed into the insulated cavity via a screw feeding piston in the lower cavity part, and it is simultaneously heated by both the direct concentrated solar radiation and the emitted IR radiation from the cavity walls. Another advantage of this kind of reactor is a low distance between the reduction zone in the cavity and the outlet evacuation zone connected to the particle filtration system, which alleviates the recombination reaction. The metallic fine powders (Zn or SnO) recovered in the filter at the outlet contain ~40% of reduced species for ZnO and ~70% for SnO_2, under an operating total pressure of about 20 kPa with a solar-to-chemical energy conversion efficiency of about 2–3%.

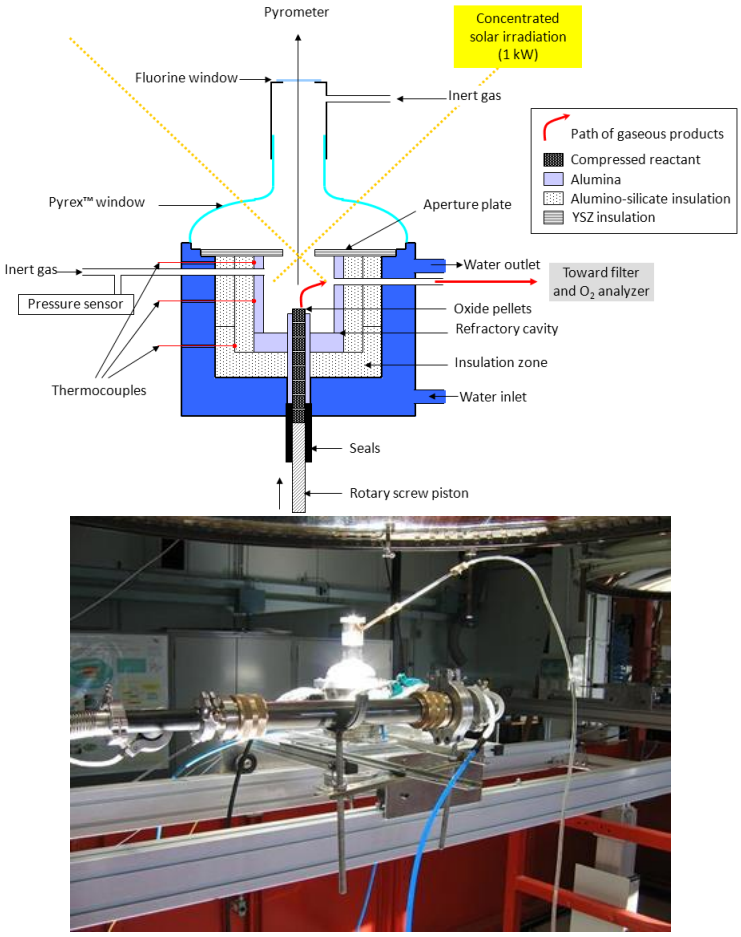

Figure 13. Solar reactor prototype designed and tested for the thermal dissociation of volatile oxides (ZnO, SnO_2) with continuous reactant injection in the form of compressed pellets.

With the objective to integrate heat between both cycle steps and to warrant continuous operation, two different reactors with moving solid oxide reactant were developed, enabling an integrated flow and transport of the reacting solid from one reaction chamber to the other. The "CR5" concept (named Counter-Rotating-Ring Receiver/Reactor/Recuperator, Figure 14a) involves two chambers separated by a stack of rotating rings [210]. The rotation drives the ring surface coated with metal oxide (ferrites) from the reduction zone to the oxidation zone. The hot part that exits the reduction zone of one reheats the entering colder parts of its two neighbors, thus enabling heat recovery (30%). The challenge and limitation of this concept reside in this assembly of rings, which must also ensure an efficient gas-tight separation of the two chambers' atmosphere. Though the concept was experimentally tested with a prototype involving cobalt ferrites, the available data are not sufficient to really assess its actual efficiency.

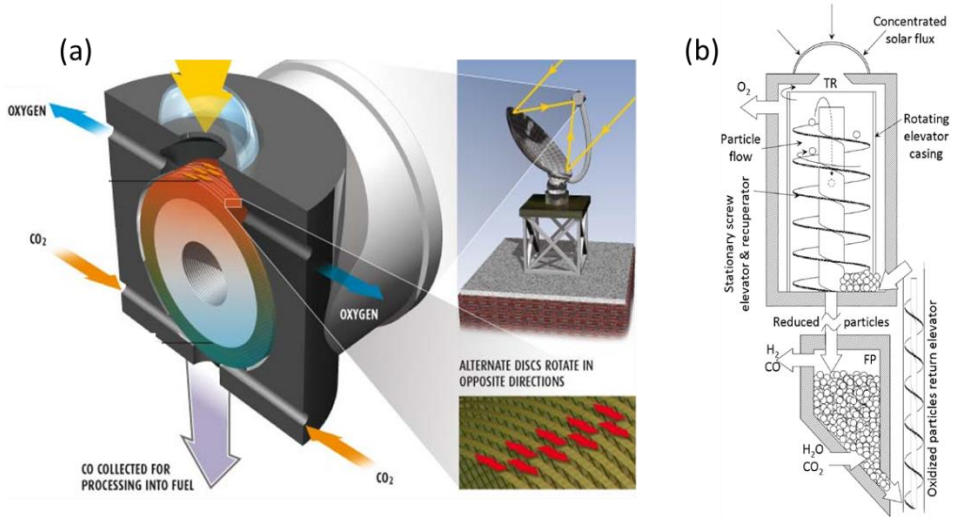

Figure 14. Scheme of integrated reactors with solid oxide displacement between redox steps: (**a**) Diagram of CR5 reactor; (**b**) Prototype of circulating dense bed reactor.

In the other concept (Figure 14b) [211], the particles are driven by a stationary screw towards the upper part of the reactor where they are subjected to concentrated radiation. Due to gravity, they go back down through the hollow axis of the screw, which acts as a heat exchanger between upward and downward particles, to the re-oxidation chamber. The authors highlight the possibility for it to continuously operate, unlike the fluidized bed, which allows a batch operation. This concept was, however, not proven, and achieving tightness due to stacked particles seems difficult, similar to the transportation of particles to the high temperature zone.

5. Conclusions

The production of green hydrogen from water-splitting and the utilization/valorization/recycling of CO_2 by thermochemical cycles coupled to a concentrated solar energy source is a relevant and attractive approach. Solar radiations are converted into heat with a reasonable efficiency, then this energy is directly used to supply the required heat to the thermochemical cycle. This allows a higher global energy efficiency for the conversion of the solar resource into fuel in comparison with the paths involving photons or electricity as intermediate sources of energy. An overview of the most suitable and advanced thermochemical redox cycles was provided and the associated solar reactor technologies applicable to H_2O and CO_2 splitting were described. Each system was discussed and critically analyzed, highlighting its advantages and drawbacks depending on the type of redox materials involved, with focus on limitations and possible methods to improve their performance (e.g., doping with other metals, control of morphology and microstructure, etc.).

- The volatile oxide cycles offer the advantages of relatively high specific fuel productivity due to discrete oxidation state transitions (leading to high oxygen amounts being released and recovered at each cycle), and of their specific surface area being renewed during each cycle thanks to the vaporization/condensation mechanism. However, it is difficult to prevent products' recombination during gas cooling in the reduction step. ZnO/Zn and SnO_2/SnO thermochemical cycles are the most attractive (with potential maximum fuel productivity up to ~12.3 mmol/g for ZnO and 6.7 mmol/g for SnO_2).
- Non-volatile oxide cycles mainly relate to non-stoichiometric oxides. They allow a lower reduction step temperature, absence of phase change during cycling, and the possibility to carry out the two reactions of the cycle in the same reactor without any reactant transfer. However, they feature a lower mass-specific fuel productivity (in the range 0.1–0.4 mmol/g) than for the stoichiometric oxides (due to a limited amount of oxygen being exchanged during solid-state reactions, as represented by the lattice

oxygen sub-stoichiometry δ), a possible loss of specific surface area during the cycling (due to sintering), and the need to optimize the formulations and the methods for the materials synthesis.

The first materials being investigated were iron-based, but due to the limitations related to their deactivation or their low mass-specific fuel productivity, research studies on ceria (CeO_2), either doped or not, are particularly active due to a high reactivity of the material with H_2O or CO_2 with high fuel production rates and thermochemical cycling stability. More recently, the ABO_3 perovskite materials are particularly attracting attention due to a significant potential for development related to their attractive redox properties (larger sub-stoichiometry accessible thanks to the oxygen mobility in comparison to pure ceria) and to many possibilities of various formulations (high flexibility offering the possibility to incorporate many dopants). The oxygen transport properties in cerium- and perovskite-based materials are particularly exploited in the H_2O and CO_2 splitting cycles. Research studies are being pursued in various fields pertaining to the formulation (selection of chemical/crystalline characteristics), materials synthesis, and shaping (elaboration of stable macroscopic porous structures during cycling) for their integration in solar reactors.

The typical solar reactors applicable for each reaction system were described, including either single chamber reactors, with both steps being performed alternately in the same reactor, or decoupled reactors, with solid reactant transfer between reaction steps. Extreme operating conditions (including very high temperatures and radiative fluxes, reducing/oxidizing atmospheres) and the requirement to manage thermal losses should be considered in the design and development of solar receivers/reactors with the ultimate aim to optimize their energy and thermochemical (solar-to-fuel) efficiencies.

Identification or discovery of new materials with large oxygen exchange capabilities, rapid chemical kinetics and stability, and their integration in efficient solar reactors are essential. Further advancements in redox material properties' characterization and performance optimization, along with innovative reactors' design, are still of critical importance to make this technology commercially viable. Finally, the thermochemical process scale-up and integration in concentrated solar plants must be taken into account for the synthesis of clean solar fuels relying exclusively on the water and carbon dioxide splitting.

Funding: This research received no external funding.

Data Availability Statement: Not applicable.

Conflicts of Interest: The authors declare no conflict of interest.

References

1. Safari, F.; Dincer, I. A Review and Comparative Evaluation of Thermochemical Water Splitting Cycles for Hydrogen Production. *Energy Convers. Manag.* **2020**, *205*, 112182. [CrossRef]
2. Rozzi, E.; Minuto, F.D.; Lanzini, A.; Leone, P. Green Synthetic Fuels: Renewable Routes for the Conversion of Non-Fossil Feedstocks into Gaseous Fuels and Their End Uses. *Energies* **2020**, *13*, 420. [CrossRef]
3. Mao, Y.; Gao, Y.; Dong, W.; Wu, H.; Song, Z.; Zhao, X.; Sun, J.; Wang, W. Hydrogen Production via a Two-Step Water Splitting Thermochemical Cycle Based on Metal Oxide—A Review. *Appl. Energy* **2020**, *267*, 114860. [CrossRef]
4. Davis, S.J.; Lewis, N.S.; Shaner, M.; Aggarwal, S.; Arent, D.; Azevedo, I.L.; Benson, S.M.; Bradley, T.; Brouwer, J.; Chiang, Y.-M.; et al. Net-Zero Emissions Energy Systems. *Science* **2018**, *360*, eaas9793. [CrossRef] [PubMed]
5. Fedunik-Hofman, L.; Bayon, A.; Donne, S.W. Comparative Kinetic Analysis of $CaCO_3$/CaO Reaction System for Energy Storage and Carbon Capture. *Appl. Sci.* **2019**, *9*, 4601. [CrossRef]
6. Ji, G.; Yang, H.; Memon, M.Z.; Gao, Y.; Qu, B.; Fu, W.; Olguin, G.; Zhao, M.; Li, A. Recent Advances on Kinetics of Carbon Dioxide Capture Using Solid Sorbents at Elevated Temperatures. *Appl. Energy* **2020**, *267*, 114874. [CrossRef]
7. Cheng, W.-H.; de la Calle, A.; Atwater, H.A.; Stechel, E.B.; Xiang, C. Hydrogen from Sunlight and Water: A Side-by-Side Comparison between Photoelectrochemical and Solar Thermochemical Water-Splitting. *ACS Energy Lett.* **2021**, *6*, 3096–3113. [CrossRef]
8. Boretti, A. Technology Readiness Level of Solar Thermochemical Splitting Cycles. *ACS Energy Lett.* **2021**, *6*, 1170–1174. [CrossRef]
9. Carrillo, R.J.; Scheffe, J.R. Advances and Trends in Redox Materials for Solar Thermochemical Fuel Production. *Sol. Energy* **2017**, *156*, 3–20. [CrossRef]

10. Kumaravel, V.; Bartlett, J.; Pillai, S.C. Photoelectrochemical Conversion of Carbon Dioxide (CO_2) into Fuels and Value-Added Products. *ACS Energy Lett.* **2020**, *5*, 486–519. [CrossRef]
11. Yaashikaa, P.R.; Senthil Kumar, P.; Varjani, S.J.; Saravanan, A. A Review on Photochemical, Biochemical and Electrochemical Transformation of CO_2 into Value-Added Products. *J. CO2 Util.* **2019**, *33*, 131–147. [CrossRef]
12. Chuayboon, S.; Abanades, S. An Overview of Solar Decarbonization Processes, Reacting Oxide Materials, and Thermochemical Reactors for Hydrogen and Syngas Production. *Int. J. Hydrogen Energy* **2020**, *45*, 25783–25810. [CrossRef]
13. Krenzke, P.T.; Fosheim, J.R.; Davidson, J.H. Solar Fuels via Chemical-Looping Reforming. *Sol. Energy* **2017**, *156*, 48–72. [CrossRef]
14. Bulfin, B.; Vieten, J.; Agrafiotis, C.; Roeb, M.; Sattler, C. Applications and Limitations of Two Step Metal Oxide Thermochemical Redox Cycles; a Review. *J. Mater. Chem. A* **2017**, *5*, 18951–18966. [CrossRef]
15. Li, S.; Wheeler, V.M.; Kumar, A.; Venkataraman, M.B.; Muhich, C.L.; Hao, Y.; Lipiński, W. Thermodynamic Guiding Principles for Designing Nonstoichiometric Redox Materials for Solar Thermochemical Fuel Production: Ceria, Perovskites, and Beyond. *Energy Technol.* **2021**, *10*, 2000925. [CrossRef]
16. Romero, M.; Steinfeld, A. Concentrating Solar Thermal Power and Thermochemical Fuels. *Energy Environ. Sci.* **2012**, *5*, 9234. [CrossRef]
17. Jensen, R.; Lyman, J.; King, J.; Guettler, R. Solar Reduction of CO2. U.S. Patent US6066187A, 23 May 2000.
18. Bhatta, S.; Nagassou, D.; Mohsenian, S.; Trelles, J.P. Photo-Thermochemical Decomposition of Carbon-Dioxide in a Direct Solar Receiver-Reactor. *Sol. Energy* **2019**, *178*, 201–214. [CrossRef]
19. Bhatta, S.; Nagassou, D.; Trelles, J.P. Solar Photo-Thermochemical Reactor Design for Carbon Dioxide Processing. *Sol. Energy* **2017**, *142*, 253–266. [CrossRef]
20. Funk, J.E.; Reinstrom, R.M. Energy Requirements in Production of Hydrogen from Water. *Ind. Eng. Chem. Proc. Des. Dev.* **1966**, *5*, 336–342. [CrossRef]
21. Abanades, S.; Charvin, P.; Flamant, G.; Neveu, P. Screening of Water-Splitting Thermochemical Cycles Potentially Attractive for Hydrogen Production by Concentrated Solar Energy. *Energy* **2006**, *31*, 2805–2822. [CrossRef]
22. Wijewardane, S. Inventions, Innovations and New Technologies—Solar Thermochemical Fuels. *Sol. Compass* **2022**, *2*, 100024. [CrossRef]
23. Agrafiotis, C.; Roeb, M.; Sattler, C. A Review on Solar Thermal Syngas Production via Redox Pair-Based Water/Carbon Dioxide Splitting Thermochemical Cycles. *Renew. Sustain. Energy Rev.* **2015**, *42*, 254–285. [CrossRef]
24. Muhich, C.L.; Ehrhart, B.D.; Al-Shankiti, I.; Ward, B.J.; Musgrave, C.B.; Weimer, A.W. A Review and Perspective of Efficient Hydrogen Generation via Solar Thermal Water Splitting: A Review and Perspective of Efficient Hydrogen Generation. *WIREs Energy Environ.* **2016**, *5*, 261–287. [CrossRef]
25. Charvin, P.; Abanades, S.; Lemort, F.; Flamant, G. Analysis of Solar Chemical Processes for Hydrogen Production from Water Splitting Thermochemical Cycles. *Energy Convers. Manag.* **2008**, *49*, 1547–155610. [CrossRef]
26. Graf, D.; Monnerie, N.; Roeb, M.; Schmitz, M.; Sattler, C. Economic Comparison of Solar Hydrogen Generation by Means of Thermochemical Cycles and Electrolysis. *Int. J. Hydrogen Energy* **2008**, *33*, 4511–4519. [CrossRef]
27. Yadav, D.; Banerjee, R. A Review of Solar Thermochemical Processes. *Renew. Sustain. Energy Rev.* **2016**, *54*, 497–532. [CrossRef]
28. Moser, M.; Pecchi, M.; Fend, T. Techno-Economic Assessment of Solar Hydrogen Production by Means of Thermo-Chemical Cycles. *Energies* **2019**, *12*, 352. [CrossRef]
29. Onigbajumo, A.; Swarnkar, P.; Will, G.; Sundararajan, T.; Taghipour, A.; Couperthwaite, S.; Steinberg, T.; Rainey, T. Techno-Economic Evaluation of Solar-Driven Ceria Thermochemical Water-Splitting for Hydrogen Production in a Fluidized Bed Reactor. *J. Clean. Prod.* **2022**, *371*, 133303. [CrossRef]
30. Ma, Z.; Davenport, P.; Saur, G. System and Technoeconomic Analysis of Solar Thermochemical Hydrogen Production. *Renew. Energy* **2022**, *190*, 294–308. [CrossRef]
31. Prats-Salvado, E.; Monnerie, N.; Sattler, C. Synergies between Direct Air Capture Technologies and Solar Thermochemical Cycles in the Production of Methanol. *Energies* **2021**, *14*, 4818. [CrossRef]
32. Centi, G.; Perathoner, S. CO_2-Based Energy Vectors for the Storage of Solar Energy. *Greenhouse Gas Sci. Technol.* **2011**, *1*, 21–35. [CrossRef]
33. Dry, M.E. The Fischer–Tropsch Process: 1950–2000. *Catal. Today* **2002**, *71*, 227–241. [CrossRef]
34. Espinoza, R.L.; Steynberg, A.P.; Jager, B.; Vosloo, A.C. Low Temperature Fischer–Tropsch Synthesis from a Sasol Perspective. *Appl. Catal. A Gen.* **1999**, *186*, 13–26. [CrossRef]
35. Steynberg, A.P.; Espinoza, R.L.; Jager, B.; Vosloo, A.C. High Temperature Fischer–Tropsch Synthesis in Commercial Practice. *Appl. Catal. A Gen.* **1999**, *186*, 41–54. [CrossRef]
36. Abanades, S. Metal Oxides Applied to Thermochemical Water-Splitting for Hydrogen Production Using Concentrated Solar Energy. *ChemEngineering* **2019**, *3*, 63. [CrossRef]
37. Scheffe, J.R.; Steinfeld, A. Oxygen Exchange Materials for Solar Thermochemical Splitting of H_2O and CO_2: A Review. *Mater. Today* **2014**, *17*, 341–348. [CrossRef]
38. Xiao, L.; Wu, S.-Y.; Li, Y.-R. Advances in Solar Hydrogen Production via Two-Step Water-Splitting Thermochemical Cycles Based on Metal Redox Reactions. *Renew. Energy* **2012**, *41*, 1–12. [CrossRef]
39. Li, X.; Sun, X.; Song, Q.; Yang, Z.; Wang, H.; Duan, Y. A Critical Review on Integrated System Design of Solar Thermochemical Water-Splitting Cycle for Hydrogen Production. *Int. J. Hydrogen Energy* 2022, *in press*. [CrossRef]

40. Oudejans, D.; Offidani, M.; Constantinou, A.; Albonetti, S.; Dimitratos, N.; Bansode, A. A Comprehensive Review on Two-Step Thermochemical Water Splitting for Hydrogen Production in a Redox Cycle. *Energies* **2022**, *15*, 3044. [CrossRef]
41. Roeb, M.; Neises, M.; Monnerie, N.; Call, F.; Simon, H.; Sattler, C.; Schmücker, M.; Pitz-Paal, R. Materials-Related Aspects of Thermochemical Water and Carbon Dioxide Splitting: A Review. *Materials* **2012**, *5*, 2015–2054. [CrossRef]
42. Gálvez, M.E.; Loutzenhiser, P.G.; Hischier, I.; Steinfeld, A. CO_2 Splitting via Two-Step Solar Thermochemical Cycles with Zn/ZnO and FeO/Fe3O4 Redox Reactions: Thermodynamic Analysis. *Energy Fuels* **2008**, *22*, 3544–3550. [CrossRef]
43. Falter, C.; Sizmann, A. Solar Thermochemical Hydrogen Production in the USA. *Sustainability* **2021**, *13*, 7804. [CrossRef]
44. Falter, C.; Scharfenberg, N.; Habersetzer, A. Geographical Potential of Solar Thermochemical Jet Fuel Production. *Energies* **2020**, *13*, 802. [CrossRef]
45. Falter, C.; Valente, A.; Habersetzer, A.; Iribarren, D.; Dufour, J. An Integrated Techno-Economic, Environmental and Social Assessment of the Solar Thermochemical Fuel Pathway. *Sustain. Energy Fuels* **2020**, *4*, 3992–4002. [CrossRef]
46. Steinfeld, A. Solar Hydrogen Production via a Two-Step Water-Splitting Thermochemical Cycle Based on Zn/ZnO Redox Reactions. *Int. J. Hydrogen Energy* **2002**, *27*, 611–619. [CrossRef]
47. Loutzenhiser, P.G.; Meier, A.; Steinfeld, A. Review of the Two-Step H_2O/CO_2-Splitting Solar Thermochemical Cycle Based on Zn/ZnO Redox Reactions. *Materials* **2010**, *3*, 4922–4938. [CrossRef]
48. Schunk, L.O.; Steinfeld, A. Kinetics of the Thermal Dissociation of ZnO Exposed to Concentrated Solar Irradiation Using a Solar-Driven Thermogravimeter in the 1800-2100 K Range. *AIChE J.* **2009**, *55*, 1497–1504. [CrossRef]
49. Levêque, G.; Abanades, S. Design and Operation of a Solar-Driven Thermogravimeter for High Temperature Kinetic Analysis of Solid–Gas Thermochemical Reactions in Controlled Atmosphere. *Sol. Energy* **2014**, *105*, 225–235. [CrossRef]
50. Levêque, G.; Abanades, S. Investigation of Thermal and Carbothermal Reduction of Volatile Oxides (ZnO, SnO_2, GeO_2, and MgO) via Solar-Driven Vacuum Thermogravimetry for Thermochemical Production of Solar Fuels. *Thermochim. Acta* **2015**, *605*, 86–94. [CrossRef]
51. Levêque, G.; Abanades, S. Kinetic Analysis of High-Temperature Solid–Gas Reactions by an Inverse Method Applied to ZnO and SnO_2 Solar Thermal Dissociation. *Chem. Eng. J.* **2013**, *217*, 139–149. [CrossRef]
52. Perkins, C.; Lichty, P.; Weimer, A.W. Determination of Aerosol Kinetics of Thermal ZnO Dissociation by Thermogravimetry. *Chem. Eng. Sci.* **2007**, *62*, 5952–5962. [CrossRef]
53. Perkins, C.; Lichty, P.R.; Weimer, A.W. Thermal ZnO Dissociation in a Rapid Aerosol Reactor as Part of a Solar Hydrogen Production Cycle. *Int. J. Hydrogen Energy* **2008**, *33*, 499–510. [CrossRef]
54. Chambon, M.; Abanades, S.; Flamant, G. Solar Thermal Reduction of ZnO and SnO_2 Characterization of the Recombination Reaction with O_2. *Chem. Eng. Sci.* **2010**, *65*, 3671–3680. [CrossRef]
55. Ernst, F.; Steinfeld, A.; Pratsinis, S. Hydrolysis Rate of Submicron Zn Particles for Solar H_2 Synthesis. *Int. J. Hydrogen Energy* **2009**, *34*, 1166–1175. [CrossRef]
56. Abanades, S. Thermogravimetry Analysis of CO_2 and H_2O Reduction from Solar Nanosized Zn Powder for Thermochemical Fuel Production. *Ind. Eng. Chem. Res.* **2012**, *51*, 741–750. [CrossRef]
57. Weibel, D.; Jovanovic, Z.R.; Gálvez, E.; Steinfeld, A. Mechanism of Zn Particle Oxidation by H_2O and CO_2 in the Presence of ZnO. *Chem. Mater.* **2014**, *26*, 6486–6495. [CrossRef] [PubMed]
58. Chambon, M.; Abanades, S.; Flamant, G. Kinetic Investigation of Hydrogen Generation from Hydrolysis of SnO and Zn Solar Nanopowders. *Int. J. Hydrogen Energy* **2009**, *34*, 5326–5336. [CrossRef]
59. Lv, M.; Zhou, J.; Yang, W.; Cen, K. Thermogravimetric Analysis of the Hydrolysis of Zinc Particles. *Int. J. Hydrogen Energy* **2010**, *35*, 2617–2621. [CrossRef]
60. Abanades, S.; Chambon, M. CO_2 Dissociation and Upgrading from Two-Step Solar Thermochemical Processes Based on ZnO/Zn and SnO_2/SnO Redox Pairs. *Energy Fuels* **2010**, *24*, 6667–6674. [CrossRef]
61. Loutzenhiser, P.G.; Barthel, F.; Stamatiou, A.; Steinfeld, A. CO_2 Reduction with Zn Particles in a Packed-Bed Reactor. *AIChE J.* **2011**, *57*, 2529–2534. [CrossRef]
62. Loutzenhiser, P.G.; Gálvez, M.E.; Hischier, I.; Stamatiou, A.; Frei, A.; Steinfeld, A. CO_2 Splitting via Two-Step Solar Thermochemical Cycles with Zn/ZnO and FeO/Fe_3O_4 Redox Reactions II: Kinetic Analysis. *Energy Fuels* **2009**, *23*, 2832–2839. [CrossRef]
63. Stamatiou, A.; Loutzenhiser, P.G.; Steinfeld, A. Solar Syngas Production via H_2O/CO_2-Splitting Thermochemical Cycles with Zn/ZnO and FeO/Fe_3O_4 Redox Reactions. *Chem. Mater.* **2010**, *22*, 851–859. [CrossRef]
64. Melchior, T.; Piatkowski, N.; Steinfeld, A. H_2 Production by Steam-Quenching of Zn Vapor in a Hot-Wall Aerosol Flow Reactor. *Chem. Eng. Sci.* **2009**, *64*, 1095–1101. [CrossRef]
65. Venstrom, L.J.; Hilsen, P.; Davidson, J.H. Heterogeneous Oxidation of Zinc Vapor by Steam and Mixtures of Steam and Carbon Dioxide. *Chem. Eng. Sci.* **2018**, *183*, 223–230. [CrossRef]
66. Lindemer, M.D.; Advani, S.G.; Prasad, A.K. Experimental Investigation of Heterogeneous Hydrolysis with Zn Vapor under a Temperature Gradient. *Int. J. Hydrogen Energy* **2017**, *42*, 7847–7856. [CrossRef]
67. Wieckert, C.; Frommherz, U.; Kräupl, S.; Guillot, E.; Olalde, G.; Epstein, M.; Santén, S.; Osinga, T.; Steinfeld, A. A 300 kW Solar Chemical Pilot Plant for the Carbothermic Production of Zinc. *J. Sol. Energy Eng.* **2007**, *129*, 190–196. [CrossRef]
68. Kräupl, S.; Steinfeld, A. Operational Performance of a 5-KW Solar Chemical Reactor for the Co-Production of Zinc and Syngas. *J. Sol. Energy Eng.* **2003**, *125*, 124–126. [CrossRef]

69. Chuayboon, S.; Abanades, S. Thermochemical Performance Assessment of Solar Continuous Methane-Driven ZnO Reduction for Co-Production of Pure Zinc and Hydrogen-Rich Syngas. *Chem. Eng. J.* **2022**, *429*, 132356. [CrossRef]
70. Chuayboon, S.; Abanades, S. Solar-Driven Chemical Looping Methane Reforming Using ZnO Oxygen Carrier for Syngas and Zn Production in a Cavity-Type Solar Reactor. *Catalysts* **2020**, *10*, 1356. [CrossRef]
71. Chuayboon, S.; Abanades, S. Combined ZnO Reduction and Methane Reforming for Co-Production of Pure Zn and Syngas in a Prototype Solar Thermochemical Reactor. *Fuel Process. Technol.* **2021**, *211*, 106572. [CrossRef]
72. Osinga, T.; Frommherz, U.; Steinfeld, A.; Wieckert, C. Experimental Investigation of the Solar Carbothermic Reduction of ZnO Using a Two-Cavity Solar Reactor. *J. Sol. Energy Eng.* **2004**, *126*, 633–637. [CrossRef]
73. Chuayboon, S.; Abanades, S. Solar Carbo-Thermal and Methano-Thermal Reduction of MgO and ZnO for Metallic Powder and Syngas Production by Green Extractive Metallurgy. *Processes* **2022**, *10*, 154. [CrossRef]
74. Chuayboon, S.; Abanades, S. Solar Metallurgy for Sustainable Zn and Mg Production in a Vacuum Reactor Using Concentrated Sunlight. *Sustainability* **2020**, *12*, 6709. [CrossRef]
75. Chuayboon, S.; Abanades, S.; Rodat, S. Solar Chemical Looping Gasification of Biomass with the ZnO/Zn Redox System for Syngas and Zinc Production in a Continuously-Fed Solar Reactor. *Fuel* **2018**, *215*, 66–79. [CrossRef]
76. Chuayboon, S.; Abanades, S. Thermodynamic and Experimental Investigation of Solar-Driven Biomass Pyro-Gasification Using H_2O, CO_2, or ZnO Oxidants for Clean Syngas and Metallurgical Zn Production. *Processes* **2021**, *9*, 687. [CrossRef]
77. Osinga, T.; Olalde, G.; Steinfeld, A. Solar Carbothermal Reduction of ZnO: Shrinking Packed-Bed Reactor Modeling and Experimental Validation. *Ind. Eng. Chem. Res.* **2004**, *43*, 7981–7988. [CrossRef]
78. Charvin, P.; Abanades, S.; Lemont, F.; Flamant, G. Experimental Study of SnO_2/SnO/Sn Thermochemical Systems for Solar Production of Hydrogen. *AIChE J.* **2008**, *54*, 2759–2767. [CrossRef]
79. Abanades, S.; Charvin, P.; Lemont, F.; Flamant, G. Novel Two-Step SnO2/SnO Water-Splitting Cycle for Solar Thermochemical Production of Hydrogen. *Int. J. Hydrogen Energy* **2008**, *33*, 6021–6030. [CrossRef]
80. Abanades, S. CO_2 and H_2O Reduction by Solar Thermochemical Looping Using SnO_2/SnO Redox Reactions: Thermogravimetric Analysis. *Int. J. Hydrogen Energy* **2012**, *37*, 8223–8231. [CrossRef]
81. Levêque, G.; Abanades, S.; Jumas, J.-C.; Olivier-Fourcade, J. Characterization of Two-Step Tin-Based Redox System for Thermochemical Fuel Production from Solar-Driven CO_2 and H_2O Splitting Cycle. *Ind. Eng. Chem. Res.* **2014**, *53*, 5668–5677. [CrossRef]
82. Levêque, G.; Abanades, S. Thermodynamic and Kinetic Study of the Carbothermal Reduction of SnO_2 for Solar Thermochemical Fuel Generation. *Energy Fuels* **2014**, *28*, 1396–1405. [CrossRef]
83. Bhosale, R.R.; Kumar, A.; Sutar, P. Thermodynamic Analysis of Solar Driven SnO_2/SnO Based Thermochemical Water Splitting Cycle. *Energy Convers. Manag.* **2017**, *135*, 226–235. [CrossRef]
84. Chambon, M.; Abanades, S.; Flamant, G. Thermal Dissociation of Compressed ZnO and SnO_2 Powders in a Moving-Front Solar Thermochemical Reactor. *AIChE J.* **2011**, *57*, 2264–2273. [CrossRef]
85. Nakamura, T. Hydrogen Production from Water Utilizing Solar Heat at High Temperatures. *Sol. Energy* **1977**, *19*, 467–475. [CrossRef]
86. Charvin, P.; Abanades, S.; Flamant, G.; Lemort, F. Two-Step Water Splitting Thermochemical Cycle Based on Iron Oxide Redox Pair for Solar Hydrogen Production. *Energy* **2007**, *32*, 1124–1133. [CrossRef]
87. Abanades, S.; Villafan-Vidales, H.I. CO_2 and H_2O Conversion to Solar Fuels via Two-Step Solar Thermochemical Looping Using Iron Oxide Redox Pair. *Chem. Eng. J.* **2011**, *175*, 368–375. [CrossRef]
88. Abanades, S.; Villafan-Vidales, I. CO_2 Valorisation Based on Fe_3O_4/FeO Thermochemical Redox Reactions Using Concentrated Solar Energy. *Int. J. Energy Res.* **2013**, *37*, 598–608. [CrossRef]
89. Tamaura, Y.; Ueda, Y.; Matsunami, J.; Hasegawa, N.; Nezuka, M.; Sano, T.; Tsuji, M. Solar Hydrogen Production by Using Ferrites. *Sol. Energy* **1999**, *65*, 55–57. [CrossRef]
90. Coker, E.N.; Ambrosini, A.; Miller, J.E. Compositional and Operational Impacts on the Thermochemical Reduction of CO_2 to CO by Iron Oxide/Yttria-Stabilized Zirconia. *RSC Adv.* **2021**, *11*, 1493–1502. [CrossRef]
91. Abanades, S.; Flamant, G. Thermochemical Hydrogen Production from a Two-Step Solar-Driven Water-Splitting Cycle Based on Cerium Oxides. *Sol. Energy* **2006**, *80*, 1611–1623. [CrossRef]
92. Charvin, P.; Abanades, S.; Beche, E.; Lemont, F.; Flamant, G. Hydrogen Production from Mixed Cerium Oxides via Three-Step Water-Splitting Cycles. *Solid State Ion.* **2009**, *180*, 1003–1010. [CrossRef]
93. Le Gal, A.; Abanades, S. Catalytic Investigation of Ceria-Zirconia Solid Solutions for Solar Hydrogen Production. *Int. J. Hydrogen Energy* **2011**, *36*, 4739–4748. [CrossRef]
94. Haeussler, A.; Abanades, S.; Jouannaux, J.; Drobek, M.; Ayral, A.; Julbe, A. Recent Progress on Ceria Doping and Shaping Strategies for Solar Thermochemical Water and CO_2 Splitting Cycles. *AIMS Mater. Sci.* **2019**, *6*, 657–684. [CrossRef]
95. Call, F.; Roeb, M.; Schmücker, M.; Sattler, C.; Pitz-Paal, R. Ceria Doped with Zirconium and Lanthanide Oxides to Enhance Solar Thermochemical Production of Fuels. *J. Phys. Chem. C* **2015**, *119*, 6929–6938. [CrossRef]
96. Roeb, M.; Säck, J.-P.; Rietbrock, P.; Prahl, C.; Schreiber, H.; Neises, M.; de Oliveira, L.; Graf, D.; Ebert, M.; Reinalter, W.; et al. Test Operation of a 100kW Pilot Plant for Solar Hydrogen Production from Water on a Solar Tower. *Sol. Energy* **2011**, *85*, 634–644. [CrossRef]

97. Fresno, F.; Fernández-Saavedra, R.; Belén Gómez-Mancebo, M.; Vidal, A.; Sánchez, M.; Isabel Rucandio, M.; Quejido, A.J.; Romero, M. Solar Hydrogen Production by Two-Step Thermochemical Cycles: Evaluation of the Activity of Commercial Ferrites. *Int. J. Hydrogen Energy* **2009**, *34*, 2918–2924. [CrossRef]
98. Lorentzou, S.; Dimitrakis, D.; Zygogianni, A.; Karagiannakis, G.; Konstandopoulos, A.G. Thermochemical H_2O and CO_2 Splitting Redox Cycles in a $NiFe_2O_4$ Structured Redox Reactor: Design, Development and Experiments in a High Flux Solar Simulator. *Sol. Energy* **2017**, *155*, 1462–1481. [CrossRef]
99. Kostoglou, M.; Lorentzou, S.; Konstandopoulos, A.G. Improved Kinetic Model for Water Splitting Thermochemical Cycles Using Nickel Ferrite. *Int. J. Hydrogen Energy* **2014**, *39*, 6317–6327. [CrossRef]
100. Guene Lougou, B.; Geng, B.; Jiang, B.; Zhang, H.; Sun, Q.; Shuai, Y.; Qu, Z.; Zhao, J.; Wang, C.-H. Copper Ferrite and Cobalt Oxide Two-Layer Coated Macroporous SiC Substrate for Efficient CO_2-Splitting and Thermochemical Energy Conversion. *J. Colloid Interface Sci.* **2022**, *627*, 516–531. [CrossRef]
101. Cho, H.S.; Gokon, N.; Kodama, T.; Kang, Y.H.; Lee, H.J. Improved Operation of Solar Reactor for Two-Step Water-Splitting H_2 Production by Ceria-Coated Ceramic Foam Device. *Int. J. Hydrogen Energy* **2015**, *40*, 114–124. [CrossRef]
102. Gokon, N.; Hasegawa, T.; Takahashi, S.; Kodama, T. Thermochemical Two-Step Water-Splitting for Hydrogen Production Using Fe-YSZ Particles and a Ceramic Foam Device. *Energy* **2008**, *33*, 1407–1416. [CrossRef]
103. Gokon, N.; Murayama, H.; Nagasaki, A.; Kodama, T. Thermochemical Two-Step Water Splitting Cycles by Monoclinic ZrO2-Supported NiFe2O4 and Fe3O4 Powders and Ceramic Foam Devices. *Sol. Energy* **2009**, *83*, 527–537. [CrossRef]
104. Chueh, W.C.; Haile, S.M. A Thermochemical Study of Ceria: Exploiting an Old Material for New Modes of Energy Conversion and CO_2 Mitigation. *Philos. Trans. R. Soc. A* **2010**, *368*, 3269–3294. [CrossRef]
105. Chueh, W.C.; Haile, S.M. Ceria as a Thermochemical Reaction Medium for Selectively Generating Syngas or Methane from H_2O and CO_2. *ChemSusChem* **2009**, *2*, 735–739. [CrossRef] [PubMed]
106. Chueh, W.C.; Falter, C.; Abbott, M.; Scipio, D.; Furler, P.; Haile, S.M.; Steinfeld, A. High-Flux Solar-Driven Thermochemical Dissociation of CO_2 and H_2O Using Nonstoichiometric Ceria. *Science* **2010**, *330*, 1797–1801. [CrossRef] [PubMed]
107. Bulfin, B.; Call, F.; Lange, M.; Lübben, O.; Sattler, C.; Pitz-Paal, R.; Shvets, I.V. Thermodynamics of CeO_2 Thermochemical Fuel Production. *Energy Fuels* **2015**, *29*, 1001–1009. [CrossRef]
108. Lu, Y.; Zhu, L.; Agrafiotis, C.; Vieten, J.; Roeb, M.; Sattler, C. Solar Fuels Production: Two-Step Thermochemical Cycles with Cerium-Based Oxides. *Prog. Energy Combust. Sci.* **2019**, *75*, 100785. [CrossRef]
109. Bhosale, R.R.; Takalkar, G.; Sutar, P.; Kumar, A.; AlMomani, F.; Khraisheh, M. A Decade of Ceria Based Solar Thermochemical H_2O/CO_2 Splitting Cycle. *Int. J. Hydrogen Energy* **2019**, *44*, 34–60. [CrossRef]
110. Rhodes, N.R.; Bobek, M.M.; Allen, K.M.; Hahn, D.W. Investigation of Long Term Reactive Stability of Ceria for Use in Solar Thermochemical Cycles. *Energy* **2015**, *89*, 924–931. [CrossRef]
111. Takalkar, G.D.; Bhosale, R.R.; Kumar, A.; AlMomani, F.; Khraisheh, M.; Shakoor, R.A.; Gupta, R.B. Transition Metal Doped Ceria for Solar Thermochemical Fuel Production. *Sol. Energy* **2018**, *172*, 204–211. [CrossRef]
112. Takalkar, G.; Bhosale, R.R.; Rashid, S.; AlMomani, F.; Shakoor, R.A.; Al Ashraf, A. Application of Li-, Mg-, Ba-, Sr-, Ca-, and Sn-Doped Ceria for Solar-Driven Thermochemical Conversion of Carbon Dioxide. *J. Mater. Sci.* **2020**, *55*, 11797–11807. [CrossRef]
113. Zhu, L.; Lu, Y.; Li, F. Reactivity of Ni, Cr and Zr Doped Ceria in CO_2 Splitting for CO Production via Two-Step Thermochemical Cycle. *Int. J. Hydrogen Energy* **2018**, *43*, 13754–13763. [CrossRef]
114. Zhu, L.; Lu, Y. Reactivity and Efficiency of Ceria-Based Oxides for Solar CO_2 Splitting via Isothermal and Near-Isothermal Cycles. *Energy Fuels* **2018**, *32*, 736–746. [CrossRef]
115. Bhosale, R.R.; Kumar, A.; AlMomani, F.; Ghosh, U.; Al-Muhtaseb, S.; Gupta, R.; Alxneit, I. Assessment of $CeZrHfO_2$ Based Oxides as Potential Solar Thermochemical CO_2 Splitting Materials. *Ceram. Int.* **2016**, *42*, 9354–9362. [CrossRef]
116. Bhosale, R.R.; Takalkar, G.D. Nanostructured Co-Precipitated Ce0.9Ln0.1O2 (Ln = La, Pr, Sm, Nd, Gd, Tb, Dy, or Er) for Thermochemical Conversion of CO_2. *Ceram. Int.* **2018**, *44*, 16688–16697. [CrossRef]
117. Arifin, D.; Ambrosini, A.; Wilson, S.A.; Mandal, B.; Muhich, C.L.; Weimer, A.W. Investigation of Zr, Gd/Zr, and Pr/Zr—Doped Ceria for the Redox Splitting of Water. *Int. J. Hydrogen Energy* **2020**, *45*, 160–174. [CrossRef]
118. Portarapillo, M.; Russo, D.; Landi, G.; Luciani, G.; Di Benedetto, A. K-Doped CeO_2–ZrO_2 for CO_2 Thermochemical Catalytic Splitting. *RSC Adv.* **2021**, *11*, 39420–39427. [CrossRef]
119. Portarapillo, M.; Landi, G.; Luciani, G.; Imparato, C.; Vitiello, G.; Deorsola, F.A.; Aronne, A.; Di Benedetto, A. Redox Behavior of Potassium Doped and Transition Metal Co-Doped $Ce_{0.75}Zr_{0.25}O_2$ for Thermochemical H_2O/CO_2 Splitting. *RSC Adv.* **2022**, *12*, 14645–14654. [CrossRef]
120. Le Gal, A.; Abanades, S. Dopant Incorporation in Ceria for Enhanced Water-Splitting Activity during Solar Thermochemical Hydrogen Generation. *J. Phys. Chem. C* **2012**, *116*, 13516–13523. [CrossRef]
121. Le Gal, A.; Abanades, S.; Bion, N.; Le Mercier, T.; Harlé, V. Reactivity of Doped Ceria-Based Mixed Oxides for Solar Thermochemical Hydrogen Generation via Two-Step Water-Splitting Cycles. *Energy Fuels* **2013**, *27*, 6068–6078. [CrossRef]
122. Bulfin, B.; Call, F.; Vieten, J.; Roeb, M.; Sattler, C.; Shvets, I.V. Oxidation and Reduction Reaction Kinetics of Mixed Cerium Zirconium Oxides. *J. Phys. Chem. C* **2016**, *120*, 2027–2035. [CrossRef]
123. Pullar, R.C.; Novais, R.M.; Caetano, A.P.F.; Barreiros, M.A.; Abanades, S.; Oliveira, F.A.C. A Review of Solar Thermochemical CO_2 Splitting Using Ceria-Based Ceramics With Designed Morphologies and Microstructures. *Front. Chem.* **2019**, *7*, 34. [CrossRef] [PubMed]

124. Gladen, A.C.; Davidson, J.H. The Morphological Stability and Fuel Production of Commercial Fibrous Ceria Particles for Solar Thermochemical Redox Cycling. *Sol. Energy* **2016**, *139*, 524–532. [CrossRef]
125. Keene, D.J.; Lipiński, W.; Davidson, J.H. The Effects of Morphology on the Thermal Reduction of Nonstoichiometric Ceria. *Chem. Eng. Sci.* **2014**, *111*, 231–243. [CrossRef]
126. Venstrom, L.J.; Petkovich, N.; Rudisill, S.; Stein, A.; Davidson, J.H. The Effects of Morphology on the Oxidation of Ceria by Water and Carbon Dioxide. *J. Sol. Energy Eng.* **2011**, *134*, 011005. [CrossRef]
127. Furler, P.; Scheffe, J.; Marxer, D.; Gorbar, M.; Bonk, A.; Vogt, U.; Steinfeld, A. Thermochemical CO_2 Splitting *via* Redox Cycling of Ceria Reticulated Foam Structures with Dual-Scale Porosities. *Phys. Chem. Chem. Phys.* **2014**, *16*, 10503–10511. [CrossRef]
128. Orfila, M.; Sanz, D.; Linares, M.; Molina, R.; Sanz, R.; Marugán, J.; Botas, J.Á. H_2 Production by Thermochemical Water Splitting with Reticulated Porous Structures of Ceria-Based Mixed Oxide Materials. *Int. J. Hydrogen Energy* **2021**, *46*, 17458–17471. [CrossRef]
129. Lorentzou, S.; Pagkoura, C.; Zygogianni, A.; Karagiannakis, G.; Konstandopoulos, A.G. Thermochemical Cycles over Redox Structured Reactors. *Int. J. Hydrogen Energy* **2017**, *42*, 19664–19682. [CrossRef]
130. Haeussler, A.; Abanades, S.; Julbe, A.; Jouannaux, J.; Drobek, M.; Ayral, A.; Cartoixa, B. Remarkable Performance of Microstructured Ceria Foams for Thermochemical Splitting of H_2O and CO_2 in a Novel High–Temperature Solar Reactor. *Chem. Eng. Res. Des.* **2020**, *156*, 311–323. [CrossRef]
131. Haeussler, A.; Abanades, S.; Julbe, A.; Jouannaux, J.; Cartoixa, B. Solar Thermochemical Fuel Production from H_2O and CO_2 Splitting via Two-Step Redox Cycling of Reticulated Porous Ceria Structures Integrated in a Monolithic Cavity-Type Reactor. *Energy* **2020**, *201*, 117649. [CrossRef]
132. Oliveira, F.A.C.; Barreiros, M.A.; Abanades, S.; Caetano, A.P.F.; Novais, R.M.; Pullar, R.C. Solar Thermochemical CO_2 Splitting Using Cork-Templated Ceria Ecoceramics. *J. CO2 Util.* **2018**, *26*, 552–563. [CrossRef]
133. Oliveira, F.A.C.; Barreiros, M.A.; Haeussler, A.; Caetano, A.P.F.; Mouquinho, A.I.; Oliveira e Silva, P.M.; Novais, R.M.; Pullar, R.C.; Abanades, S. High Performance Cork-Templated Ceria for Solar Thermochemical Hydrogen Production via Two-Step Water-Splitting Cycles. *Sustain. Energy Fuels* **2020**, *4*, 3077–3089. [CrossRef]
134. Haeussler, A.; Abanades, S.; Costa Oliveira, F.A.; Barreiros, M.A.; Caetano, A.P.F.; Novais, R.M.; Pullar, R.C. Solar Redox Cycling of Ceria Structures Based on Fiber Boards, Foams, and Biomimetic Cork-Derived Ecoceramics for Two-Step Thermochemical H_2O and CO_2 Splitting. *Energy Fuels* **2020**, *34*, 9037–9049. [CrossRef]
135. Malonzo, C.D.; De Smith, R.M.; Rudisill, S.G.; Petkovich, N.D.; Davidson, J.H.; Stein, A. Wood-Templated CeO_2 as Active Material for Thermochemical CO Production. *J. Phys. Chem. C* **2014**, *118*, 26172–26181. [CrossRef]
136. Haeussler, A.; Abanades, S.; Julbe, A.; Jouannaux, J.; Cartoixa, B. Two-Step CO_2 and H_2O Splitting Using Perovskite-Coated Ceria Foam for Enhanced Green Fuel Production in a Porous Volumetric Solar Reactor. *J. CO2 Util.* **2020**, *41*, 101257. [CrossRef]
137. Abanades, S.; Haeussler, A.; Julbe, A. Synthesis and Thermochemical Redox Cycling of Porous Ceria Microspheres for Renewable Fuels Production from Solar-Aided Water-Splitting and CO_2 Utilization. *Appl. Phys. Lett.* **2021**, *119*, 023902. [CrossRef]
138. Abanades, S.; Haeussler, A.; Julbe, A. Thermochemical Solar-Driven Reduction of CO_2 into Separate Streams of CO and O_2 via an Isothermal Oxygen-Conducting Ceria Membrane Reactor. *Chem. Eng. J.* **2021**, *422*, 130026. [CrossRef]
139. Haeussler, A.; Abanades, S. Additive Manufacturing and Two-Step Redox Cycling of Ordered Porous Ceria Structures for Solar-Driven Thermochemical Fuel Production. *Chem. Eng. Sci.* **2021**, *246*, 116999. [CrossRef]
140. Abanades, S.; Haeussler, A. Two-Step Thermochemical Cycles Using Fibrous Ceria Pellets for H_2 Production and CO_2 Reduction in Packed-Bed Solar Reactors. *Sustain. Mater. Technol.* **2021**, *29*, e00328. [CrossRef]
141. Parvanian, A.M.; Salimijazi, H.; Shabaninejad, M.; Troitzsch, U.; Kreider, P.; Lipiński, W.; Saadatfar, M. Thermochemical CO_2 Splitting Performance of Perovskite Coated Porous Ceramics. *RSC Adv.* **2020**, *10*, 23049–23057. [CrossRef]
142. Hoes, M.; Ackermann, S.; Theiler, D.; Furler, P.; Steinfeld, A. Additive-Manufactured Ordered Porous Structures Made of Ceria for Concentrating Solar Applications. *Energy Technol.* **2019**, *7*, 1900484. [CrossRef]
143. Bayon, A.; de la Calle, A.; Ghose, K.K.; Page, A.; McNaughton, R. Experimental, Computational and Thermodynamic Studies in Perovskites Metal Oxides for Thermochemical Fuel Production: A Review. *Int. J. Hydrogen Energy* **2020**, *45*, 12653–12679. [CrossRef]
144. Vieten, J.; Bulfin, B.; Huck, P.; Horton, M.; Guban, D.; Zhu, L.; Lu, Y.; Persson, K.A.; Roeb, M.; Sattler, C. Materials Design of Perovskite Solid Solutions for Thermochemical Applications. *Energy Environ. Sci.* **2019**, *12*, 1369–1384. [CrossRef]
145. Kubicek, M.; Bork, A.H.; Rupp, J.L.M. Perovskite Oxides—A Review on a Versatile Material Class for Solar-to-Fuel Conversion Processes. *J. Mater. Chem. A* **2017**, *5*, 11983–12000. [CrossRef]
146. Ezbiri, M.; Takacs, M.; Theiler, D.; Michalsky, R.; Steinfeld, A. Tunable Thermodynamic Activity of La_xSr_{1-x} $Mn_yAl_{1-y}O_{3-\delta}$ ($0 \leq x \leq 1$, $0 \leq y \leq 1$) Perovskites for Solar Thermochemical Fuel Synthesis. *J. Mater. Chem. A* **2017**, *5*, 4172–4182. [CrossRef] [PubMed]
147. Emery, A.A.; Saal, J.E.; Kirklin, S.; Hegde, V.I.; Wolverton, C. High-Throughput Computational Screening of Perovskites for Thermochemical Water Splitting Applications. *Chem. Mater.* **2016**, *28*, 5621–5634. [CrossRef]
148. Gao, X.; Liu, G.; Zhu, Y.; Kreider, P.; Bayon, A.; Gengenbach, T.; Lu, T.; Liu, Y.; Hinkley, J.; Lipiński, W.; et al. Earth-Abundant Transition Metal Oxides with Extraordinary Reversible Oxygen Exchange Capacity for Efficient Thermochemical Synthesis of Solar Fuels. *Nano Energy* **2018**, *50*, 347–358. [CrossRef]

149. Gao, K.; Liu, X.; Jiang, Z.; Zheng, H.; Song, C.; Wang, X.; Tian, C.; Dang, C.; Sun, N.; Xuan, Y. Direct Solar Thermochemical CO_2 Splitting Based on Ca- and Al-Doped $SmMnO_3$ Perovskites: Ultrahigh CO Yield within Small Temperature Swing. *Renew. Energy* **2022**, *194*, 482–494. [CrossRef]
150. Gao, K.; Liu, X.; Wang, T.; Zhu, Z.; Li, P.; Zheng, H.; Song, C.; Xuan, Y.; Li, Y.; Ding, Y. Sr-Doped $SmMnO_3$ Perovskites for High-Performance near-Isothermal Solar Thermochemical CO_2-to-Fuel Conversion. *Sustain. Energy Fuels* **2021**, *5*, 4295–4310. [CrossRef]
151. Liu, X.; Wang, T.; Gao, K.; Meng, X.; Xu, Q.; Song, C.; Zhu, Z.; Zheng, H.; Hao, Y.; Xuan, Y. Ca- and Ga-Doped $LaMnO_3$ for Solar Thermochemical CO_2 Splitting with High Fuel Yield and Cycle Stability. *ACS Appl. Energy Mater.* **2021**, *4*, 9000–9012. [CrossRef]
152. Naik, J.M.; Ritter, C.; Bulfin, B.; Steinfeld, A.; Erni, R.; Patzke, G.R. Reversible Phase Transformations in Novel Ce-Substituted Perovskite Oxide Composites for Solar Thermochemical Redox Splitting of CO_2. *Adv. Energy Mater.* **2021**, *11*, 2003532. [CrossRef]
153. Ezbiri, M.; Takacs, M.; Stolz, B.; Lungthok, J.; Steinfeld, A.; Michalsky, R. Design Principles of Perovskites for Solar-Driven Thermochemical Splitting of CO_2. *J. Mater. Chem. A* **2017**, *5*, 15105–15115. [CrossRef] [PubMed]
154. Gálvez, M.E.; Jacot, R.; Scheffe, J.; Cooper, T.; Patzke, G.; Steinfeld, A. Physico-Chemical Changes in Ca, Sr and Al-Doped La–Mn–O Perovskites upon Thermochemical Splitting of CO $_2$ via Redox Cycling. *Phys. Chem. Chem. Phys.* **2015**, *17*, 6629–6634. [CrossRef] [PubMed]
155. Haeussler, A.; Abanades, S.; Jouannaux, J.; Julbe, A. Non-Stoichiometric Redox Active Perovskite Materials for Solar Thermochemical Fuel Production: A Review. *Catalysts* **2018**, *8*, 611. [CrossRef]
156. Demont, A.; Abanades, S.; Beche, E. Investigation of Perovskite Structures as Oxygen-Exchange Redox Materials for Hydrogen Production from Thermochemical Two-Step Water-Splitting Cycles. *J. Phys. Chem. C* **2014**, *118*, 12682–12692. [CrossRef]
157. Haeussler, A.; Julbe, A.; Abanades, S. Investigation of Reactive Perovskite Materials for Solar Fuel Production via Two-Step Redox Cycles: Thermochemical Activity, Thermodynamic Properties and Reduction Kinetics. *Mater. Chem. Phys.* **2022**, *276*, 125358. [CrossRef]
158. Jouannaux, J.; Haeussler, A.; Drobek, M.; Ayral, A.; Abanades, S.; Julbe, A. Lanthanum Manganite Perovskite Ceramic Powders for CO_2 Splitting: Influence of Pechini Synthesis Parameters on Sinterability and Reactivity. *Ceram. Int.* **2019**, *45*, 15636–15648. [CrossRef]
159. Sai Gautam, G.; Stechel, E.B.; Carter, E.A. Exploring Ca–Ce–M–O (M = 3d Transition Metal) Oxide Perovskites for Solar Thermochemical Applications. *Chem. Mater.* **2020**, *32*, 9964–9982. [CrossRef]
160. Barcellos, D.R.; Coury, F.G.; Emery, A.; Sanders, M.; Tong, J.; McDaniel, A.; Wolverton, C.; Kaufman, M.; O'Hayre, R. Phase Identification of the Layered Perovskite $Ce_xSr_{2-x}MnO_4$ and Application for Solar Thermochemical Water Splitting. *Inorg. Chem.* **2019**, *58*, 7705–7714. [CrossRef]
161. McDaniel, A.H. Renewable Energy Carriers Derived from Concentrating Solar Power and Nonstoichiometric Oxides. *Curr. Opin. Green Sustain. Chem.* **2017**, *4*, 37–43. [CrossRef]
162. Rao, C.N.R.; Dey, S. Generation of H_2 and CO by Solar Thermochemical Splitting of H_2O and CO_2 by Employing Metal Oxides. *J. Solid State Chem.* **2016**, *242*, 107–115. [CrossRef]
163. Dey, S.; Naidu, B.S.; Rao, C.N.R. Beneficial Effects of Substituting Trivalent Ions in the B-Site of $La_{0.5}Sr_{0.5}Mn_{1-x}A_xO_3$ (A = Al, Ga, Sc) on the Thermochemical Generation of CO and H_2 from CO_2 and H_2O. *Dalton Trans.* **2016**, *45*, 2430–2435. [CrossRef] [PubMed]
164. Qian, X.; He, J.; Mastronardo, E.; Baldassarri, B.; Wolverton, C.; Haile, S.M. Favorable Redox Thermodynamics of $SrTi_{0.5}Mn_{0.5}O_{3-\delta}$ in Solar Thermochemical Water Splitting. *Chem. Mater.* **2020**, *32*, 9335–9346. [CrossRef]
165. Qian, X.; He, J.; Mastronardo, E.; Baldassarri, B.; Yuan, W.; Wolverton, C.; Haile, S.M. Outstanding Properties and Performance of CaTi0.5Mn0.5O3−δ for Solar-Driven Thermochemical Hydrogen Production. *Matter* **2021**, *4*, 688–708. [CrossRef]
166. Demont, A.; Abanades, S. High Redox Activity of Sr-Substituted Lanthanum Manganite Perovskites for Two-Step Thermochemical Dissociation of CO_2. *RSC Adv.* **2014**, *4*, 54885–54891. [CrossRef]
167. Kildahl, H.; Cao, H.; Ding, Y. Thermochemical Splitting of Carbon Dioxide by Lanthanum Manganites-Understanding the Mechanistic Effects of Doping. *Energy Storage Sav.* 2022, *in press*. [CrossRef]
168. Bork, A.H.; Povoden-Karadeniz, E.; Carrillo, A.J.; Rupp, J.L.M. Thermodynamic Assessment of the Solar-to-Fuel Performance of La0.6Sr0.4Mn1-YCryO3-Delta Perovskite Solid Solution Series. *Acta Mater.* **2019**, *178*, 163–172. [CrossRef]
169. Carrillo, A.J.; Kim, K.J.; Hood, Z.D.; Bork, A.H.; Rupp, J.L.M. $La_{0.6}Sr_{0.4}Cr_{0.8}Co_{0.2}O_3$ Perovskite Decorated with Exsolved Co Nanoparticles for Stable CO_2 Splitting and Syngas Production. *ACS Appl. Energy Mater.* **2020**, *3*, 4569–4579. [CrossRef]
170. Sawaguri, H.; Gokon, N.; Hayashi, K.; Iwamura, Y.; Yasuhara, D. Two-Step Thermochemical CO_2 Splitting Using Partially-Substituted Perovskite Oxides of La0.7Sr0.3Mn0.9X0.1O3 for Solar Fuel Production. *Front. Energy Res.* **2022**, *10*, 872959. [CrossRef]
171. Gager, E.; Frye, M.; McCord, D.; Scheffe, J.; Nino, J.C. Reticulated Porous Lanthanum Strontium Manganite Structures for Solar Thermochemical Hydrogen Production. *Int. J. Hydrogen Energy* **2022**, *47*, 31152–31164. [CrossRef]
172. Sastre, D.; Carrillo, A.J.; Serrano, D.P.; Pizarro, P.; Coronado, J.M. Exploring the Redox Behavior of La0.6Sr0.4Mn1−xAlxO3 Perovskites for CO_2-Splitting in Thermochemical Cycles. *Top. Catal.* **2017**, *60*, 1108–1118. [CrossRef]
173. Luciani, G.; Landi, G.; Aronne, A.; Di Benedetto, A. Partial Substitution of B Cation in $La_{0.6}Sr_{0.4}MnO_3$ Perovskites: A Promising Strategy to Improve the Redox Properties Useful for Solar Thermochemical Water and Carbon Dioxide Splitting. *Sol. Energy* **2018**, *171*, 1–7. [CrossRef]
174. Wang, L.; Al-Mamun, M.; Liu, P.; Wang, Y.; Yang, H.G.; Zhao, H. Notable Hydrogen Production on LaxCa1−xCoO3 Perovskites via Two-Step Thermochemical Water Splitting. *J. Mater. Sci.* **2018**, *53*, 6796–6806. [CrossRef]

175. Orfila, M.; Linares, M.; Molina, R.; Botas, J.Á.; Sanz, R.; Marugán, J. Perovskite Materials for Hydrogen Production by Thermochemical Water Splitting. *Int. J. Hydrogen Energy* **2016**, *41*, 19329–19338. [CrossRef]
176. Takacs, M.; Hoes, M.; Caduff, M.; Cooper, T.; Scheffe, J.R.; Steinfeld, A. Oxygen Nonstoichiometry, Defect Equilibria, and Thermodynamic Characterization of $LaMnO_3$ Perovskites with Ca/Sr A-Site and Al B-Site Doping. *Acta Mater.* **2016**, *103*, 700–710. [CrossRef]
177. Demont, A.; Abanades, S. Solar Thermochemical Conversion of CO_2 into Fuel via Two-Step Redox Cycling of Non-Stoichiometric Mn-Containing Perovskite Oxides. *J. Mater. Chem. A* **2015**, *3*, 3536–3546. [CrossRef]
178. Nair, M.M.; Abanades, S. Insights into the Redox Performance of Non-Stoichiometric Lanthanum Manganite Perovskites for Solar Thermochemical CO_2 Splitting. *ChemistrySelect* **2016**, *1*, 4449–4457. [CrossRef]
179. Nair, M.M.; Abanades, S. Experimental Screening of Perovskite Oxides as Efficient Redox Materials for Solar Thermochemical CO_2 Conversion. *Sustain. Energy Fuels* **2018**, *2*, 843–854. [CrossRef]
180. Heo, S.J.; Sanders, M.; O'Hayre, R.; Zakutayev, A. Double-Site Substitution of Ce into (Ba, Sr)MnO_3 Perovskites for Solar Thermochemical Hydrogen Production. *ACS Energy Lett.* **2021**, *6*, 3037–3043. [CrossRef]
181. Carrillo, A.J.; Bork, A.H.; Moser, T.; Sediva, E.; Hood, Z.D.; Rupp, J.L.M. Modifying $La_{0.6}Sr_{0.4}MnO_3$ Perovskites with Cr Incorporation for Fast Isothermal CO_2-Splitting Kinetics in Solar-Driven Thermochemical Cycles. *Adv. Energy Mater.* **2019**, *9*, 1803886. [CrossRef]
182. McDaniel, A.H.; Miller, E.C.; Arifin, D.; Ambrosini, A.; Coker, E.N.; O'Hayre, R.; Chueh, W.C.; Tong, J. Sr- and Mn-Doped LaAlO3−δ for Solar Thermochemical H_2 and CO Production. *Energy Environ. Sci.* **2013**, *6*, 2424. [CrossRef]
183. Şanlı, S.B.; Pişkin, B. Effect of B-Site Al Substitution on Hydrogen Production of La0.4Sr0.6Mn1-XAlx (X = 0.4, 0.5 and 0.6) Perovskite Oxides. *Int. J. Hydrogen Energy* **2022**, *47*, 19411–19421. [CrossRef]
184. Cooper, T.; Scheffe, J.R.; Galvez, M.E.; Jacot, R.; Patzke, G.; Steinfeld, A. Lanthanum Manganite Perovskites with Ca/Sr A-Site and Al B-Site Doping as Effective Oxygen Exchange Materials for Solar Thermochemical Fuel Production. *Energy Technol.* **2015**, *3*, 1130–1142. [CrossRef]
185. Carrillo, R.J.; Scheffe, J.R. Beyond Ceria: Theoretical Investigation of Isothermal and Near-Isothermal Redox Cycling of Perovskites for Solar Thermochemical Fuel Production. *Energy Fuels* **2019**, *33*, 12871–12884. [CrossRef]
186. Nair, M.M.; Abanades, S. Solid-State Reoxidation Kinetics of A/B-Site Substituted $LaMnO_3$ During Solar Thermochemical CO_2 Conversion. *Energy Technol.* **2021**, *9*, 2000885. [CrossRef]
187. Nair, M.M.; Abanades, S. Correlating Oxygen Mobility with Thermochemical CO_2-Splitting Efficiency in A-Site Substituted Manganite Perovskites. *Sustain. Energy Fuels* **2021**, *5*, 4570–4574. [CrossRef]
188. Kodama, T.; Bellan, S.; Gokon, N.; Cho, H.S. Particle Reactors for Solar Thermochemical Processes. *Sol. Energy* **2017**, *156*, 113–132. [CrossRef]
189. Abanades, S.; Rodat, S.; Boujjat, H. Solar Thermochemical Green Fuels Production: A Review of Biomass Pyro-Gasification, Solar Reactor Concepts and Modelling Methods. *Energies* **2021**, *14*, 1494. [CrossRef]
190. Alonso, E.; Romero, M. Review of Experimental Investigation on Directly Irradiated Particles Solar Reactors. *Renew. Sustain. Energy Rev.* **2015**, *41*, 53–67. [CrossRef]
191. Gokon, N.; Takahashi, S.; Yamamoto, H.; Kodama, T. Thermochemical Two-Step Water-Splitting Reactor with Internally Circulating Fluidized Bed for Thermal Reduction of Ferrite Particles. *Int. J. Hydrogen Energy* **2008**, *33*, 2189–2199. [CrossRef]
192. Al-Shankiti, I.; Ehrhart, B.D.; Weimer, A.W. Isothermal Redox for H_2O and CO_2 Splitting—A Review and Perspective. *Sol. Energy* **2017**, *156*, 21–29. [CrossRef]
193. Davenport, T.C.; Yang, C.-K.; Kucharczyk, C.J.; Ignatowich, M.J.; Haile, S.M. Maximizing Fuel Production Rates in Isothermal Solar Thermochemical Fuel Production. *Appl. Energy* **2016**, *183*, 1098–1111. [CrossRef]
194. Hao, Y.; Yang, C.-K.; Haile, S.M. High-Temperature Isothermal Chemical Cycling for Solar-Driven Fuel Production. *Phys. Chem. Chem. Phys.* **2013**, *15*, 17084. [CrossRef] [PubMed]
195. Hoskins, A.L.; Millican, S.L.; Czernik, C.E.; Alshankiti, I.; Netter, J.C.; Wendelin, T.J.; Musgrave, C.B.; Weimer, A.W. Continuous On-Sun Solar Thermochemical Hydrogen Production via an Isothermal Redox Cycle. *Appl. Energy* **2019**, *249*, 368–376. [CrossRef]
196. Kong, H.; Hao, Y.; Jin, H. Isothermal versus Two-Temperature Solar Thermochemical Fuel Synthesis: A Comparative Study. *Appl. Energy* **2018**, *228*, 301–308. [CrossRef]
197. Ma, T.; Wang, L.; Chang, C.; Akhatov, J.S.; Fu, M.; Li, X. A Comparative Thermodynamic Analysis of Isothermal and Non-Isothermal CeO_2-Based Solar Thermochemical Cycle with Methane-Driven Reduction. *Renew. Energy* **2019**, *143*, 915–921. [CrossRef]
198. Venstrom, L.J.; De Smith, R.M.; Hao, Y.; Haile, S.M.; Davidson, J.H. Efficient Splitting of CO_2 in an Isothermal Redox Cycle Based on Ceria. *Energy Fuels* **2014**, *28*, 2732–2742. [CrossRef]
199. Haeussler, A.; Chuayboon, S.; Abanades, S. Solar Redox Cycling of Ceria in a Monolithic Reactor for Two-Step H_2O/CO_2 Splitting: Isothermal Methane-Induced Reduction versus Temperature-Swing Cycle. *AIP Conf. Proc.* **2020**, *2303*, 170009. [CrossRef]
200. Ben-Arfa, B.A.E.; Abanades, S.; Salvado, I.M.M.; Ferreira, J.M.F.; Pullar, R.C. Robocasting of 3D Printed and Sintered Ceria Scaffold Structures with Hierarchical Porosity for Solar Thermochemical Fuel Production from the Splitting of CO_2. *Nanoscale* **2022**, *14*, 4994–5001. [CrossRef]
201. Haeussler, A.; Abanades, S.; Jouannaux, J.; Julbe, A. Demonstration of a Ceria Membrane Solar Reactor Promoted by Dual Perovskite Coatings for Continuous and Isothermal Redox Splitting of CO_2 and H_2O. *J. Membr. Sci.* **2021**, *634*, 119387. [CrossRef]

202. Tou, M.; Michalsky, R.; Steinfeld, A. Solar-Driven Thermochemical Splitting of CO_2 and In Situ Separation of CO and O_2 across a Ceria Redox Membrane Reactor. *Joule* **2017**, *1*, 146–154. [CrossRef]
203. Tou, M.; Jin, J.; Hao, Y.; Steinfeld, A.; Michalsky, R. Solar-Driven Co-Thermolysis of CO_2 and H_2O Promoted by *in Situ* Oxygen Removal across a Non-Stoichiometric Ceria Membrane. *React. Chem. Eng.* **2019**, *4*, 1431–1438. [CrossRef]
204. Wu, X.-Y.; Ghoniem, A.F. Mixed Ionic-Electronic Conducting (MIEC) Membranes for Thermochemical Reduction of CO_2: A Review. *Prog. Energy Combust. Sci.* **2019**, *74*, 1–30. [CrossRef]
205. Charvin, P.; Abanades, S.; Neveu, P.; Lemont, F.; Flamant, G. Dynamic Modeling of a Volumetric Solar Reactor for Volatile Metal Oxide Reduction. *Chem. Eng. Res. Des.* **2008**, *86*, 1216–1222. [CrossRef]
206. Koepf, E.; Villasmil, W.; Meier, A. Pilot-Scale Solar Reactor Operation and Characterization for Fuel Production via the Zn/ZnO Thermochemical Cycle. *Appl. Energy* **2016**, *165*, 1004–1023. [CrossRef]
207. Abanades, S.; Charvin, P.; Flamant, G. Design and Simulation of a Solar Chemical Reactor for the Thermal Reduction of Metal Oxides: Case Study of Zinc Oxide Dissociation. *Chem. Eng. Sci.* **2007**, *62*, 6323–6333. [CrossRef]
208. Chambon, M.; Abanades, S.; Flamant, G. Design of a Lab-Scale Rotary Cavity-Type Solar Reactor for Continuous Thermal Dissociation of Volatile Oxides Under Reduced Pressure. *J. Sol. Energy Eng.* **2010**, *132*, 021006. [CrossRef]
209. Koepf, E.; Advani, S.G.; Steinfeld, A.; Prasad, A.K. A Novel Beam-down, Gravity-Fed, Solar Thermochemical Receiver/Reactor for Direct Solid Particle Decomposition: Design, Modeling, and Experimentation. *Int. J. Hydrogen Energy* **2012**, *37*, 16871–16887. [CrossRef]
210. Diver, R.B.; Miller, J.E.; Allendorf, M.D.; Siegel, N.P.; Hogan, R.E. Solar Thermochemical Water-Splitting Ferrite-Cycle Heat Engines. *J. Sol. Energy Eng.* **2008**, *130*, 041001. [CrossRef]
211. Ermanoski, I.; Siegel, N.P.; Stechel, E.B. A New Reactor Concept for Efficient Solar-Thermochemical Fuel Production. *J. Sol. Energy Eng.* **2013**, *135*, 031002. [CrossRef]